UNIVERSIDADE DA BEIRA INTERIOR

Covilhã, Portugal

Development of the Structure of a long Endurance Electric UAV

Alexandre Emanuel Guerreiro Duarte

Dissertação para obtenção do Grau de Mestre em

Engenharia Aeronáutica

(Ciclo de estudos integrado)

Orientador: Professor Doutor Pedro Vieira Gamboa

Covilhã, abril 2016

Dedication

To my beloved parents, António Duarte and Eugénia Duarte without whom I would never be where I am now. A big thank you!

To my brother, António Duarte, who helped me to beat all the difficulties in my life and to whom I wish the best of luck for his future.

To my grandparents who are for me, my second parents and to whom I am grateful for their sympathy and kindness.

To my girlfriend, Sara Alves, who is always ready to help me and for her pacience, love and compassion.

To all my family whose affection and encouragement were my source of inspiration.

"If we did all the things we are capable off,

We would literally astound ourselves."

Thomas A. Edison

Acknowledgements

Firstly, a big thank you to all my family who supported me throughout these five years away from home.

A special thank you to my supervisor Professor Pedro Gamboa for his support, technical guidance and knowledge of aircraft design.

A big thank you to Eng. Pedro Santos, for not only being a good company and a good friend during my project, but also for his tips and knowledge that he provided to me about the UAV manufacturing and the CNC machining. I will always be thankful for his support!

Another big thank you for the members of this project, Pedro Moutinho, Afonso Rodriques and Pedro Carrola who helped me on the conception of this UAV.

Thanks to my love, Sara, who was always my support along this work.

And last, but not the least, a big thank to all my friends from my hometown and those I made along this journey, especially Jonas, Ricardo, Francisco, Pedro and Gilberto.

Resumo

Este trabalho tem como objetivo o desenvolvimento e criação da estrutura de um avião não tripulado (UAV) de longa autonomia movido a energia solar.

O desenvolvimento teve como principal objetivo a criação de uma estrutura suficientemente leve, para poder efetuar diversas missões com uma carga útil de 1 Kg. A estrutura do UAV foi dividida em três partes, as quais compreendem: a fuselagem, empenagens e suporte de empenagens. Estas foram projetadas utilizando o CATIA® para verificar as interfaces e para estudar posições de acesso e funcionalidade. Dado que o objetivo principal é de uma estrutura leve, foi utilizado como material a fibra de carbono para a fuselagem e suporte de empenagens e a madeira para as empenagens.

A estrutura em compósito foi dimensionada utilizando dois métodos: método numérico e método computacional, com recurso ao *software* de elementos finitos ANSYS®.

A produção da estrutura do UAV foi executada em duas fases. A primeira foi a estrutura em compósito utilizando o método de *hand lay-up* e *vacuum baggin method*. E a segunda as estruturas das empenagens, utilizando os métodos de construção em madeira.

Produzida toda a estrutura, foram efetuados testes estruturais para verificação de todos os métodos de construção bem como da análise estrutural.

Palavras-chave

Energia solar, UAV, Voo de grande autonomia, Estruturas em compósito, Análise estrutural, Teste estrutural.

Abstract

The goal of this project is to design and create the structure of a long endurance unmanned aerial vehicle (UAV) using solar power.

The design's main requirement was the creation of a low weight structure to handle diverse missions with a 1 Kilogram of payload. The UAV structure was divided in three parts: fuselage, empennages and empennage support, designed using CATIA® to verify interfaces and to study the positioning of the systems access and functionality. Because the main target is to build a low weight structure, the carbon fibre and wood were chosen for the fuselage, empennage support and tail, respectively.

Two methods of structure analyses were used to design the composite structures, one a numerical analysis and the other the finite element method from ANSYS®.

The UAV structure was manufactured in two phases. First was the composite structure using the hand lay-up and vacuum bagging method. And the second was the empennage structure using balsa wood construction.

When the UAV structure was finished, a structural test was carried out to verify both analysis and manufacturing methods.

Keywords

Solar power, UAV, Long endurance flight, Composite structures, Structural analysis, Structural testing.

Table of Contents

List of Tables

List of Figures

List of Acronyms

ABS	Acrylonitrile butadiene styrene
CA	Aerodynamic Center
AEROG	Aeronautics and Astronautics Research Center
AR	Aspect ratio
LAETA	Associated Laboratory on Energy, Transports and Aeronautics
CG	Center of Gravity
CMC	Ceramic-matrix Composites
CS-VLA	Certification Specifications for Very Light Aeroplanes
CAD	Computer Aided Design
CAM	Computer Aided Machining Software
CNC	Computer Numerical Control
FEM	Finite Element Method
GPS	Global Positioning System
IDMEC	Institute of Mechanical Engineering
LE	Leading Edge
LEMAC	Leading edge of the MAC
MTOW	Maximum Take-off Weight
MAC	Mean Aerodynamic Chord
MMC	Metal-matrix Composites
PMC	Polymer-matrix Composites
TE	Trailing Edge
UAV	Unmanned Air Vehicle

Nomenclature

S	Area	$[m^2]$
U_{de}	Derived gust velocity	$[m/s]$
F	Force	$[N]$
K_g	Gust alleviation factor	$[-]$
L_H	Horizontal tail Lift	$[N]$
n	Load factor	$[-]$
m	Mass	$[Kg]$
$\bar{c}$	Mean aerodynamic chord	$[m]$
M	Moment	$[N.m]$
M_0	Pitching moment	$[N.m]$
K_y	Radius of gyration in roll	$[m]$
K_z	Radius of gyration in yaw	$[m]$
C_r	Root chord	$[m]$
I	Moment of inertia	$[m^4]$
S_y	Shear force on y axis	$[N]$
V	Speed	$[m/s]$
C_t	Tip chord	$[m]$
W	Weight	$[N]$
L_W	Wing Lift	$[N]$
M/S	Wing loading	$[Kg/m^2]$

Greek letters

μ_g	Aeroplane mass ratio	$[-]$
$\ddot{\theta}$	Angular acceleration in roll	$[rad/s^2]$
ρ	Density	$[Kg/m^3]$
μ_{gt}	Lateral mass ratio	$[-]$
σ	Normal stress	$[Pa]$
δ_V	Rudder deflection	[°]
τ	Shear stress	$[Pa]$
λ	Taper ratio	$[-]$
β	Yaw angle	[°]

Chapter 1: Introduction

1.1 Motivation

Nowadays the increase of Greenhouses gases (GHG) emissions is leading to global warming. The GHG emissions are mainly caused by the burning of fossil fuels which are responsible for 79.4%[1] of the GHG emissions in Europe[1].The aerospace industry currently accounts for about 3% of the total EU greenhouse emissions, but they have been increasing fast since 1990 by 87%[2]. The main factor that lead to this increase it's the reduction of the cost of aviation as a means of transportation in these past few years. It's predicted that by 2020 the global international aviation emissions may increase up to around 70% compared to 2005.

The rapid growth of aviation emissions lead to a new alternative to the fossil fuels. The solar power, which has 0% of GHG emissions, may be the proper choice[3]. This is a renewable energy source that will always be available. Nowadays it's not yet possible to use solar power on commercial airlines due the limitation of the technology in creating and storing the energy needed. But it can be used on small aircrafts of various fields for civilian or military applications. This application can be for: coastal and border surveillance, atmospherically and weather research and prediction or environmental, forestry, agricultural, and oceanic monitoring[4].

1.2 Objectives

The objectives of this work consisted in the development and construction of the structure for a Long endurance electric UAV with the follow requirements:

- To study and learn about the current design and manufacturing techniques of a generic unmanned aerial vehicle;
- To analyse the structure of the unmanned aerial vehicle;
- To design and manufacture the unmanned aerial vehicle;
- To learn practical experience through producing an unmanned aerial vehicle;
- Perform a structural test.

[1]GHG emissions in 2013.

1.3 State of Art

1.3.1 Introduction to Composites

1.3.1.1 Composite Materials

The composites are, by definition, materials composed of two or more materials that results in better properties than those of the individual components used alone. These composites are composed in matrix and reinforcements[5].

The reinforcements of the fibres carry the load exerted on the composites structures, and provide strength and stiffness. The type and the quantity will determine the final properties.

The Table 1.1 shows the typical mechanical properties of the most common fibres.

Table 1.1 - Typical mechanical properties [3]

Fibre material	Density $[Kg/m^3]$	Tensile modulus $[MPa]$	Tensile Strength $[GPa]$
Carbon	1500-2000	2000-5600	180-500
Glass	2550	3450-5000	69-84
Kevlar	1390	2750-3000	80-130
Boron	2200-2700	2750-3600	400

The matrix material has several critical functions, which includes binding the fibres in the proper orientation, transferring the load to them and also protecting it from the abrasion and the environment. They are divided in ceramic, organic or metal.

The metal matrix composites usually consist of a low-density metal, such as aluminium or magnesium, reinforced with particles of fibres or ceramic materials, such as silicon carbide or graphite. This matrix has a high range of temperature application and they have the best properties that can be achieved by conventional metallic alloys. They have a high specific strength and stiffness, low thermal expansion, good thermal stability and improved wear resistance.

The ceramic matrix composites are used in high temperatures in the limit that the metal or polymer matrixes can handle. They have several interesting properties such as, high elastic modulus, low thermal expansion, low thermal conductivity, high melting point, a good chemical and a weather resistance. But they have a low strain which is a major concern on this matrix, as it, quite often, leads to catastrophic failure.

The polymer matrix composite is the most common matrix used on aircraft structures. It is divided in thermosetting and thermoplastic polymers.

The thermosetting polymers are long-chain molecules that cure by cross-linking to a fully three-dimension network and cannot be melted and reformed. Their great advantage is that they allow fabrication of composites at relatively low temperatures and pressures since they pass through a low-viscosity stage before polymerization and crosslinking. The big disadvantage of these composites is that they can't be recycled.

On the other hand, the thermoplastic is a high-viscosity resin that is processed by heating it above its melting temperature. Because a thermoset resin sets up and cures during processing, it cannot be reprocessed by reheating.

The Table 1.2 explains the main advantages as well as the main disadvantages of the metal and ceramic matrix comparing with the organic matrix.

Table 1.2 - Comparing MMC and CMC with PMC

Matrix	Advantages	Disadvantages
MMC	-higher compressive strength -high electric and thermal conductivity; -resistant to impact damage;	-Expensive fabrication -Susceptible to corrosion, with conducting fibres.
CMC	-low conductivity -low thermal expansion; -resistant to aggressive environments.	-fabrication can be expensive and difficult; -the joining is difficult; -relatively low toughness

The fabrication techniques of the polymer composite are different than those of the thermosetting or thermoplastic composites. The most common techniques are the Wet lay-up or Spray-up; Prepreg Lay-up; Filament Winding; and Resin transfer moulding[5].

Wet Lay-up & Spray-up

The wet lay-up process is a primitive but effective method. It is generally used for prototyping and small batch production. This method uses a mould where the reinforcement is laid, one layer at a time. Catalysed resin is then worked into the reinforcement using a brush or roller. Figure 1.1-a) shows a schematic of the hand laminating process.

In the Spray-up method the resin and the fibre are sprayed onto a reusable mould. It may be applied separately or simultaneously in a combined stream from a chopper gun. Figure 1.1 –b) shows a schematic of the spray-up process.

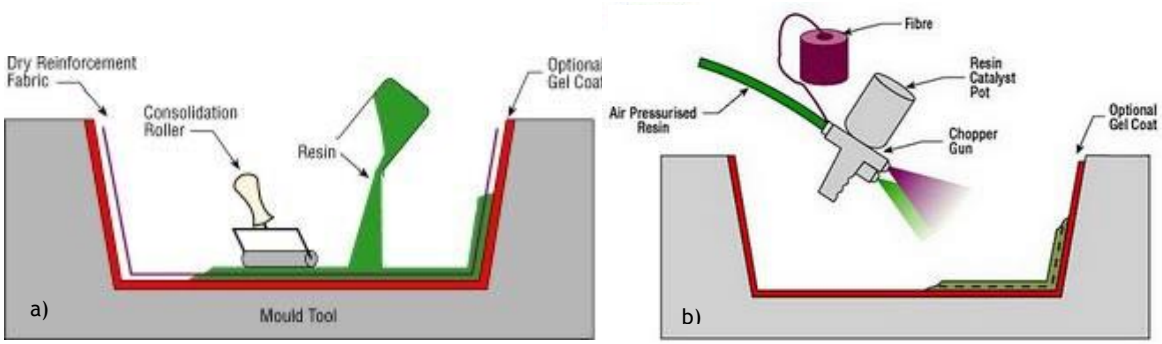

Figure 1.1 - Wet Lay-up (a) and Spray-up (b) [26].

Prepreg Lay-up

The prepreg is an identical process, as the wet lay-up. In this process the reinforcement is pre-impregnated by a supplier with a resin already containing hardener. The pre-preg are then applied to the mould in the correct position, orientation, and sequence. This is a method very often used by the aerospace industry.

Filament Winding

This process basically involves the winding of continuous fibre, impregnated with resins, over a rotating or stationary mandrel. It is widely used on surfaces of revolution, per example: the pressure vessels, missile launch tubes or fuselages.

This is a comparatively simple operation in which continuous reinforcements in the form of roving or monofilaments are wound over a rotating mandrel. Specially designed machines, traversing at speeds synchronized with the mandrel rotation, control the winding angles and the placement of the reinforcements. Figure 1.2 shows a schematic of the filament winding.

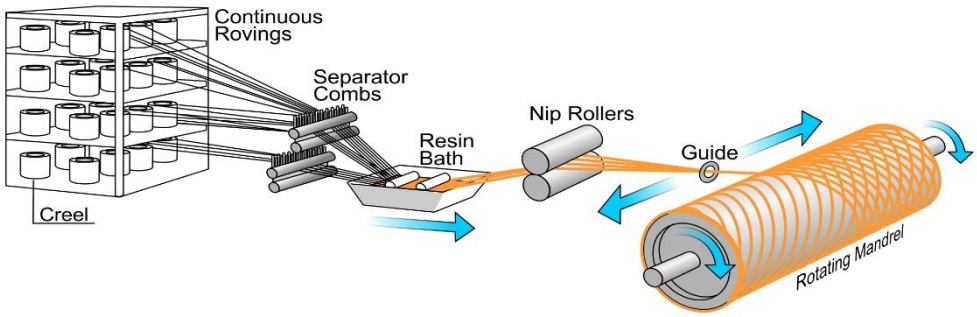

Figure 1.2 – Filament winding[27].

Resin Transfer Moulding

This RTM is a gradually common form of moulding, using liquid composites. In this process the dry fibre reinforcements are positioned on the mould, it is closed and compressed using a vacuum pump. Then a catalysed low viscosity resin is pumped into the mould, displacing the air at the edges, until it is filled. Figure 1.3 shows a schematic of the RTM.

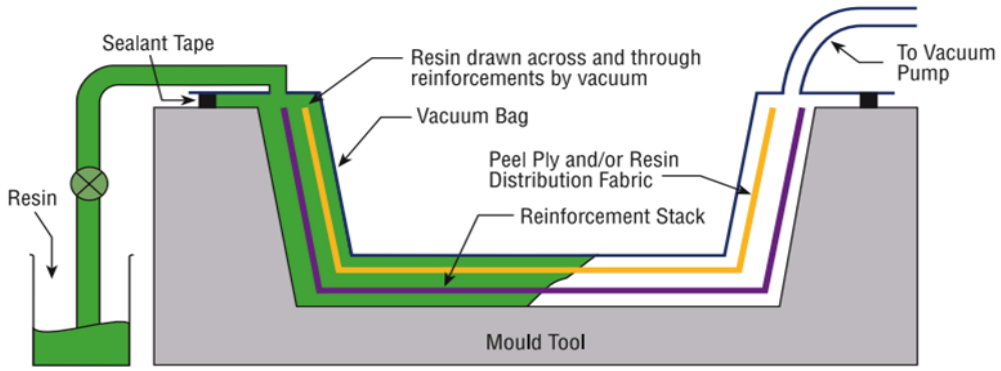

Figure 1.3 - Resin transfer moulding [28].

1.3.1.2 Composite Structures on Aeronautic

The composite structure has become an important application on aerospace industry, since its first application in the 1960s. The excellent properties of the composite materials have big advantages compared with the traditional materials. It was gradually implemented over the last years due to the high safety standards, specifically in the commercial aircraft industry.

Firstly, the composites, such as the fiberglass, were implemented on parts that don't much effect the aircraft's flying capabilities such as the interior parts, sidewalls, bag racks, and galleys. Only when the use of composites was proven successfully it was introduced into secondary aircraft structures like spoilers, rudders, ailerons, and flaps[6]. This transition provides not only a weight and a fuel consumption reduction, but also an end on the galvanic corrosion and on the structures fatigue, which is the major problem of the aluminium alloys. The Figure 1.4 shows the growth of composite fibres usage on aerospace industry. It can see that since the past 20 years the carbon fibre has increase on the percentage of material in airframe.

The new generation of aerospace composites structures, like the B-787, have already a higher percentage of carbon fibre when compared with metal. This aircraft was designed almost totally with high-performance carbon fibre materials including the wing, stabilizer and fuselage which represent 50% of the aircraft weight, Figure 1.5.

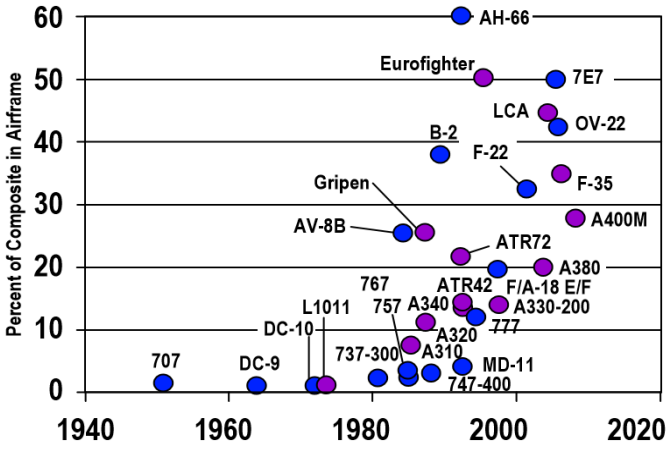

Figure 1.4 - Growth of aerospace composite structures.[30]

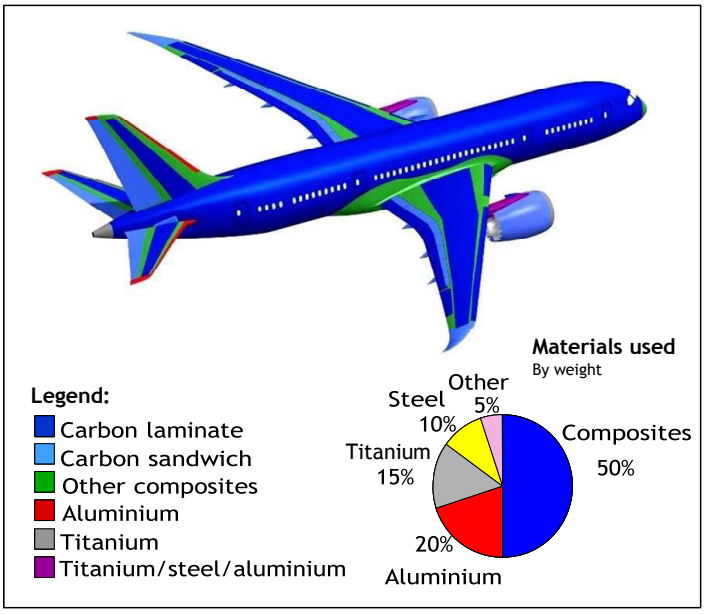

Figure 1.5 – B-787 structure [29].

1.3.2 Brief History of Unmanned Aerial Vehicles

The unmanned Aerial Vehicle (UAV) is defined as a type of powered aircraft that does not carry a human pilot and that can fly autonomously or be remotely controlled. These types of powered aircrafts started in the early 1950s, when they were used on surveillance missions or to attack all kinds of targets. Since then, the use of these kind of aircraft has increased rapidly in military and civil aviation application due to the better cost efficiency when compared to operated systems and to being multi-purpose versatile aircraft.

Due to the use of fossil fuels, which are nowadays a big problem to the society, and the need to conduct flight surveillances, or other missions, with a greater endurance a new philosophy

of UAV was born, the solar powered UAV. These UAV's have the objective to use solar radiation to propel the UAV.

The first UAV using a solar propulsion system was the Sunrise 1, made in 1974,which had 12.25 Kg of weight and 9.76 m of wingspan. It flew only 20 minutes at an altitude of 100m on his inaugural flight. An improved version was made with the same wingspan, but with weight reduced to 10.21 Kg. After some testing this version was damaged due the failure of the command and control system.

Since this early time, many more model airplane builders tried to fly with solar energy and this passion has become more and more affordable. Of course, at the beginning, the autonomy was limited only to a few seconds, but it rapidly become minutes and then hours[3].

The improvement of the composite structures and also the technology brought some new solar powered UAV's. Some of the past remarkable projects were the Pathfinder, and the AtlantikSolar UAV.

The Pathfinder project, funded by the US government, has the objective to study the feasibility of long duration flight using solar electric power. This UAV had 30 meters of wingspan and weighed 254 Kg. It accomplished its first flight in 1993 and in 1997 it set a record of altitude of 21.802 meters. An improved UAV, the Pathfinder plus, was projected with a bigger wingspan, Figure 1.5, new solar aerodynamic propulsion and system technologies.

Figure 1.5 - Pathfinder plus

The AtlantikSolar project[7], Figure 1.6, headed by ETH Zurich's Autonomous Systems was capable of performing flights with up to 10 days of duration with a 5.6 meters wingspan. The mission has the objective to cross the Atlantic Ocean optimizing a low power consumption and flight efficiency.

Figure 1.6 - AtlantikSolar UAV.

The Table 1.3 shows a resume of the UAV specifications.

Table 1.3 - UAV specifications

UAV	Wingspan $[m]$	Cruise Speed $[m/s]$	Mass $[Kg]$	Solar cells/ Power $[W]$	Primary Structure materials
Sunrise I	9.76	6.17	12.25	4096 - 450	Spruce and balsa.
Sunrise II	9.76	6.17	10.21	4480 – 600	Spruce and balsa.
Pathfinder	29.5	8.94	252	N/A - 7500	Composites, plastic, foam.
Pathfinder plus	36.3	8.94	315	N/A - 12500	Composites, plastic, foam.
Atlantik Solar	5.6	≈7.90	6.3	88 - 260[1]	Lightweight carbon fibre & Kevlar

[1] Value during the day.

1.4 Content of this thesis

This thesis concentrates on developing a UAV structure regarding the calculation, fabrication and assembly of the LEEUAV.

Chapter 2 explains the project of the Long Endurance Electric UAV and its mission requirements. It introduces the configuration of the LEEUAV regarding the systems and the structure.

Chapter 3 explains the different materials used on this project, the design features and the structure analyses.

Chapter 4 starts explaining the different methods used to manufacture the structures of the LEEUAV, like the vacuum bagging process and balsa wood construction.

Chapter 5 explains the different connections of each structure and an overall design of the final configuration of the LEEUAV.

The last chapter contemplates the project synthesis, the final considerations and the prospects for future work.

Chapter 2: Concept of the LEEUAV

2.1 Project Overview

The project of the Long Endurance Electric Unmanned Air Vehicle or LEEUAV was started by a consortium with the objective to build a vehicle capable of flying for a long time using solar power and carrying a payload of up to $1\ Kg$. This consortium has as partners the AEROG, LAETA and IDMEC.

The LEEUAV was developed to fulfil some requirements previously stipulated by the consortium: the LEEUAV needs to be hand launched; it must fly for eight hours in the equinox at a cruise speed of 7 m/s and an altitude of 1000m; its structure should fit in a typical sized car trunk to ease transportation; and it should not have a landing gear[8].This requirements also include some specifications:

- Long endurance flight using electric propulsion system and solar power cells. In particular, the use of high efficiently solar panel cells, high capacity/density batteries, an efficient compact motor and an appropriate long endurance aerodynamic design;

- Autonomous flight using an auto-pilot navigation system;

- High strength/low height structure with the use of composite materials and the critical areas like fuselage/wing capable of resisting strong impacts on landing;

- Adaptability to multiple mission profiles with a design for sufficiently large payload range capability and upgradeable modular avionics, to enable an easy software upload and/or hardware swap to meet the selected mission requirements.

The purpose of this project is to build a low cost electric UAV, fabricated using composites, mainly powered with high efficiency solar panels, capable to transport, easy to build and maintain and flexible enough to perform different missions.

2.2 Mission Requirements

The LEEUAV mission was implemented by the parameters introduced in the previous section so the mission profile is divide by five phases Figure 2.1:

1. Take-off by hand;
2. Climb up to 1000 meters;
3. Cruise flying at an altitude of 1000 meters for 8 hours during the equinox;
4. Descent without power;
5. Landing in a field.

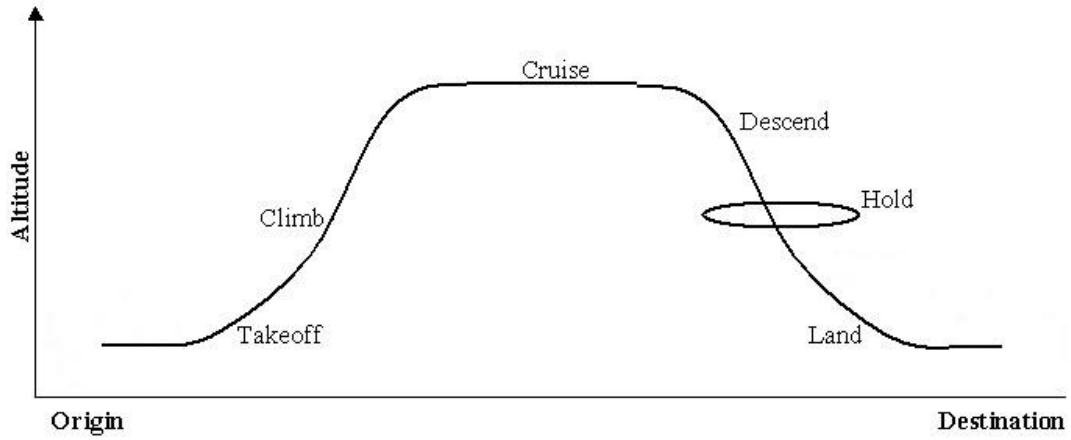

Figure 2.1 – Mission profile[31].

2.3 Conceptual Design

The conceptual design was an extensive parametric study made by Luis [9], in a spreadsheet where the primary design parameters were the mean chord and the wing span. Other parameters allowed to vary in the study were the cruise lift coefficient, the centre of gravity position, the aerofoil, the motor and the propeller.

The solution of the parametric study can be seen in Table 2.1 and Table 2.2 that shows the summary of the dimensions and weights of the LEEUAV and an estimated performance of the LEEUAV, respectively.

Table 2.1 – Summary of UAV estimated performance[9].

	Units	Value
Cruise speed	[m/s]	7.5
Design dive speed	$[m/s]$	21.1
Maximum rate of climb	[m/s]	2.2
Lift-to-drag ratio	$[-]$	20
Maximum speed	[m/s]	21.1
Stall speed	[m/s]	6.1
Take-off distance	[m]	8.1

Table 2.2 – Summary of UAV dimensions and weights[9].

	Units	Value
Span	[m]	4.500
Length	[m]	2.370
Root wing chord	[m]	0.350
Tip wing chord	[m]	0.250
Wing area	$[m^2]$	1.485
Aspect ratio	$[-]$	13.63
Horizontal tail chord	[m]	0.175
Horizontal tail span	[m]	0.700
Horizontal tail area	$[m^2]$	0.123
Vertical tail root chord	[m]	0.574
Vertical tail tip chord	[m]	0.345
Vertical tail span	$[m]$	0.280
Vertical tail area	$[m^2]$	0.129
Structure weight	[N]	16.36
Payload weight	[N]	9.81
Take-off weight	[N]	52.40
Load factor max	$[-]$	3

2.4 Configuration

2.4.1 Systems

2.4.1.1 Propulsive

The propulsive system has a huge importance to the system efficiency, so for this mission's success its necessary an appropriate motor, a solar panels, a battery and a solar charger.

The choice was the Hyperion ZS 3025-10 [10] (Figure 2.2) with a 13x8 propeller. This motor has the specifications on Table 2.3.

Table 2.3 - Hyperion ZS 3025-10 Specifications

	Units	Value
Kv	[rpm/v]	775
I_{max}	[A]	65
P_{max}	[W]	1150
Weight	[Kg]	0.1976

Figure 2.2 - Hyperion ZS 3025-10 [10].

The solar panels are the principal system to this project. The choice made was the SunPower model C60[11]. The parametric study established that the number of cells needed to perform the mission is 22 cells with a maximum power of 222W. The solar charger chosen is the Genasun GV-10[12]. This is a solar charger specifically used to a 3 cells LiPo batteries with a maximum power of 140W.

The chosen battery was a LiPo SLS APL 10,000mAh – 3S[13] and the ESC is a Castle Creation Phoenix Edge 100 A[14].

Table 2.4 – Electric Components Specifications.

Component	Weight$[Kg]$	Dimensions $[cm]$ (Length x Width x Height)
Battery	0.750	16.5 x 6.4 x 3.0
Solar charge	0.185	$14 \times 6.5 \times 3.1$

2.4.1.2 Control

The control surfaces of the UAV are actuated by servos. The servos chosen for the ailerons and elevator were the Corona DS-939MG, Figure 2.3-b, and for the rudder the TGY-225MG was chosen, Figure 2.3 -a, the specifications can be seen on Table 2.5 can be seen the specifications.

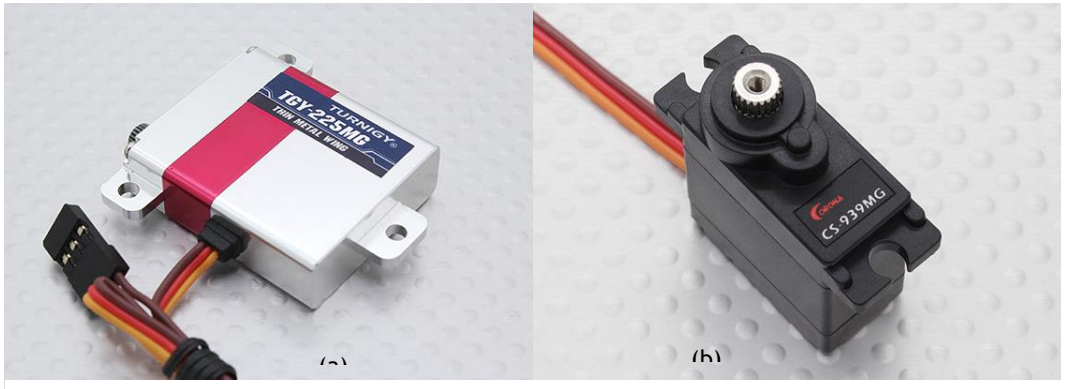

Figure 2.3 – Servo TGY-225MG(a) and Corona DS-939MG(b)

Table 2.5 - Control Components Specifications

2.4.2 Structure

The configuration of all structures of the LEEUAV use a CAD program, CATIA®[15], to design all structural components, to verify interfaces and to study the positioning of the systems balance, access and functionality.

2.4.2.1 Fuselage

The first configuration of the fuselage can be seen on Figure 2.4, in this configuration was implemented two bodies. One has the sufficient length to be launched by hand and the other to fit all equipment needed to perform the mission.

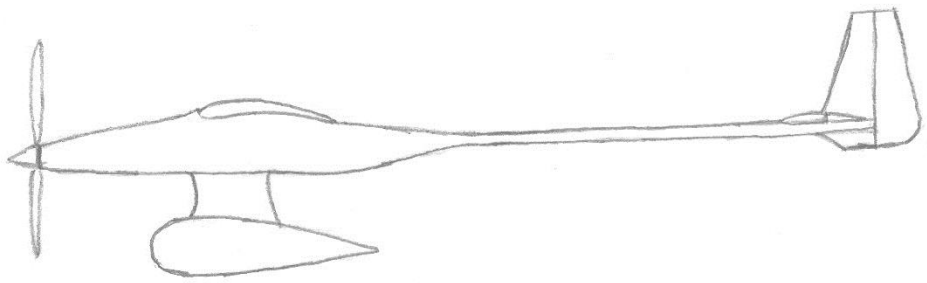

Figure 2.4 - First outline configuration of the LEEUAV [9].

During the project conception it was clear that a unique body of the fuselage have the sufficiently area to fit all the equipment needed to perform the mission and to able to be launch by hand. Figure 2.5 shows the fuselage structure with the tail tube and the empennage support. The project requirements required that the LEEUAV needs to fit on a regular car trunk so the choice was that the tube have to be removable.

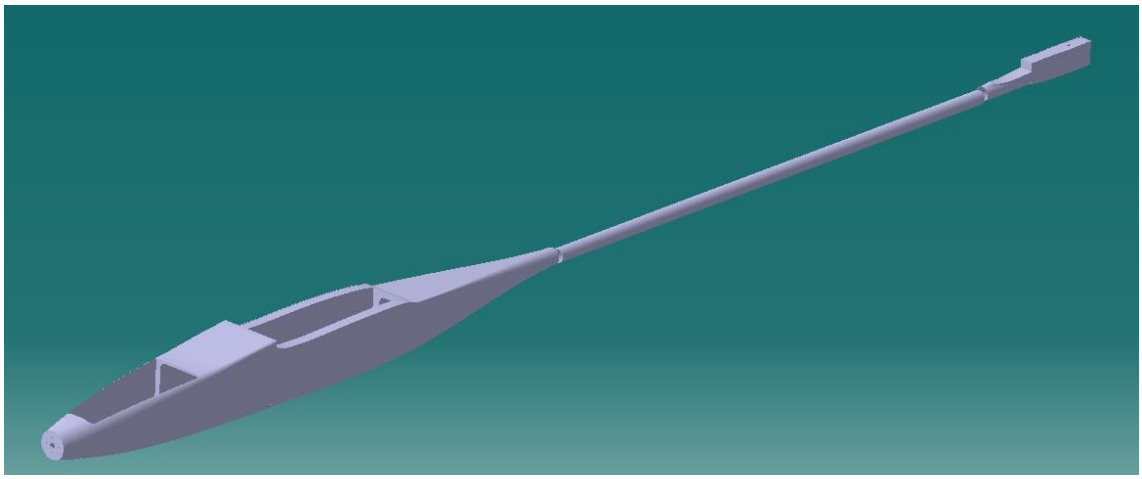

Figure 2.5 - Last version of the LEEUAV fuselage.

During the tests of the prototype the launch become dangerous due the take-off speed being close to the stall speed and due to the proximity of the propeller to the controller. The alternative was to build a trolley, Figure 2.6. This trolley will help the LEEUAV roll on the runway until the take-off.

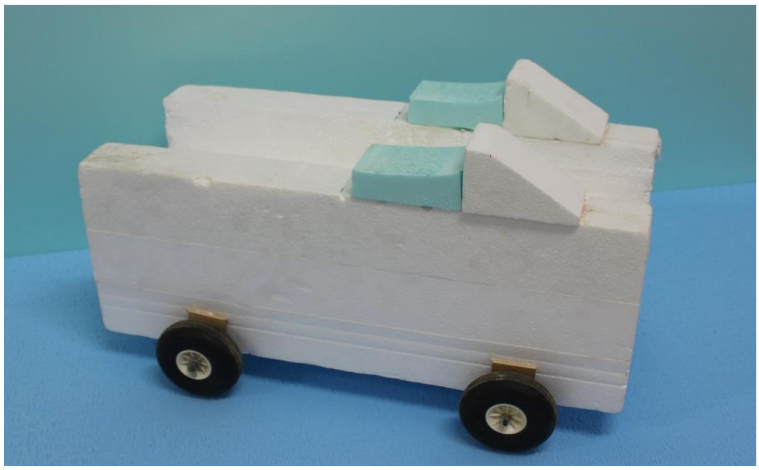

Figure 2.6 - Trolley

2.4.2.2 Tail

The LEEUAV tail has a conventional configuration, Figure 2.7, which provides the stability and control to the UAV. It is composed with two main parts: the vertical stabilizer to which the rudder is attached; and the horizontal stabilizer to which the elevator is attached with an angle of attack of $-3º$. These two structures are attached to tail support but due the mission requirements, the horizontal tail needs to be removable.

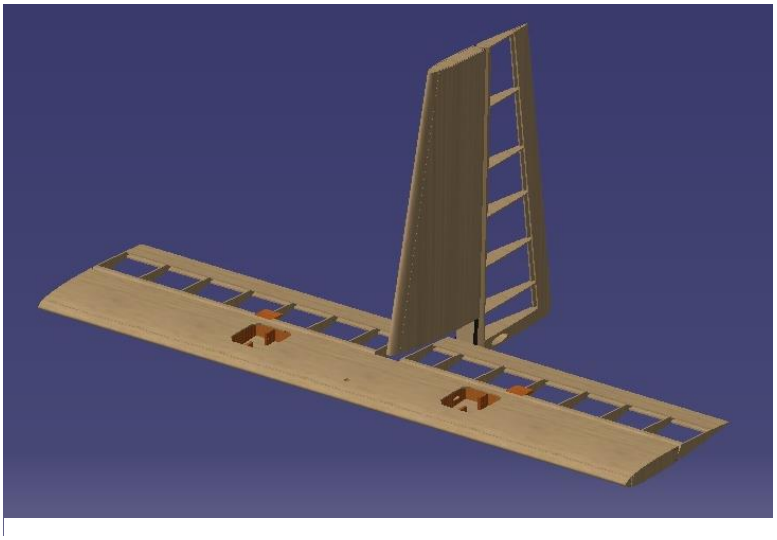

Figure 2.7 – LEEUAV tail configuration.

2.4.2.3 Wing

The LEEUAV wing has a rectangular wing configuration with an area to fit all the solar panels. It is divided in three sections capable of being disassemble for transportation. The Figure 2.8 represents the span of each wing section and also the position of the solar panels divided in four sections: two section with 12 cells, each, on central wing panel and; two other section on each wing tip with 10 cells.

The wing was already manufactured by Luis[9] with the follow configuration, visible in Figure 2.9. It also implemented the connection points with the fuselage: two carbon fibre rods, in the leading edge, and two screws in the trailing edge.

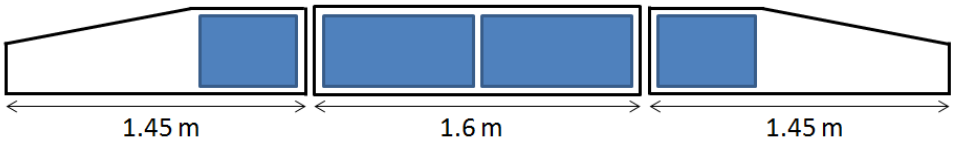

Figure 2.8 –Wing divided in three section with the position of the solar panels.

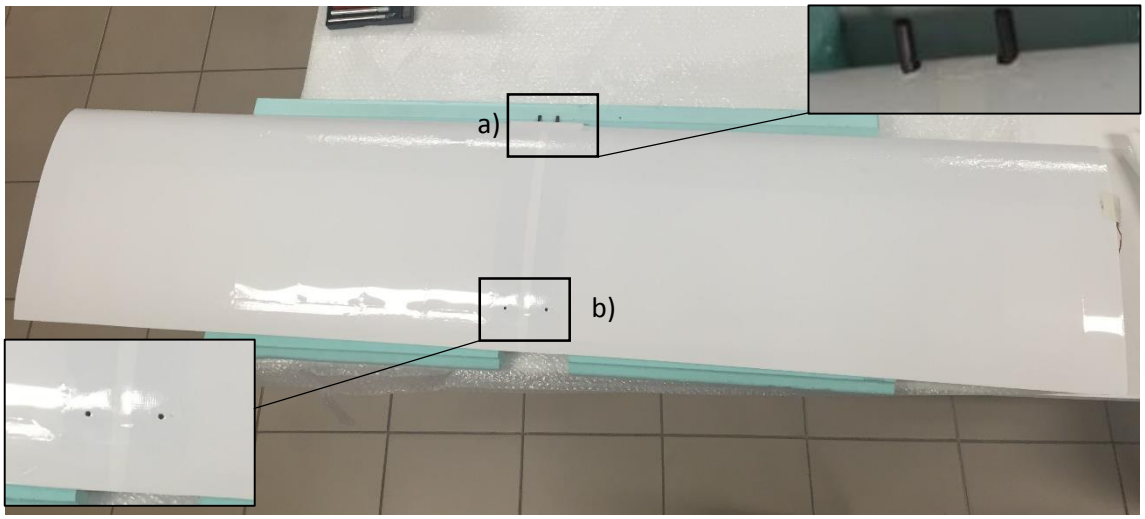

Figure 2.9 –Wing central-panel (a-carbon fibre rod; b-screws position).

2.5 CAD Drawings

The Figure 2.11 shows the top, side and front views of the UAV reflecting the results of the parametric study, the structural concept definition, the systems integration and all the alterations that were made to the project. The available area on the horizontal stabilizer or on the wing tip can be used in the future to place additional solar cells, if necessary to increase the motor power or the systems power.

The complete airframe is shown on Figure 2.10.

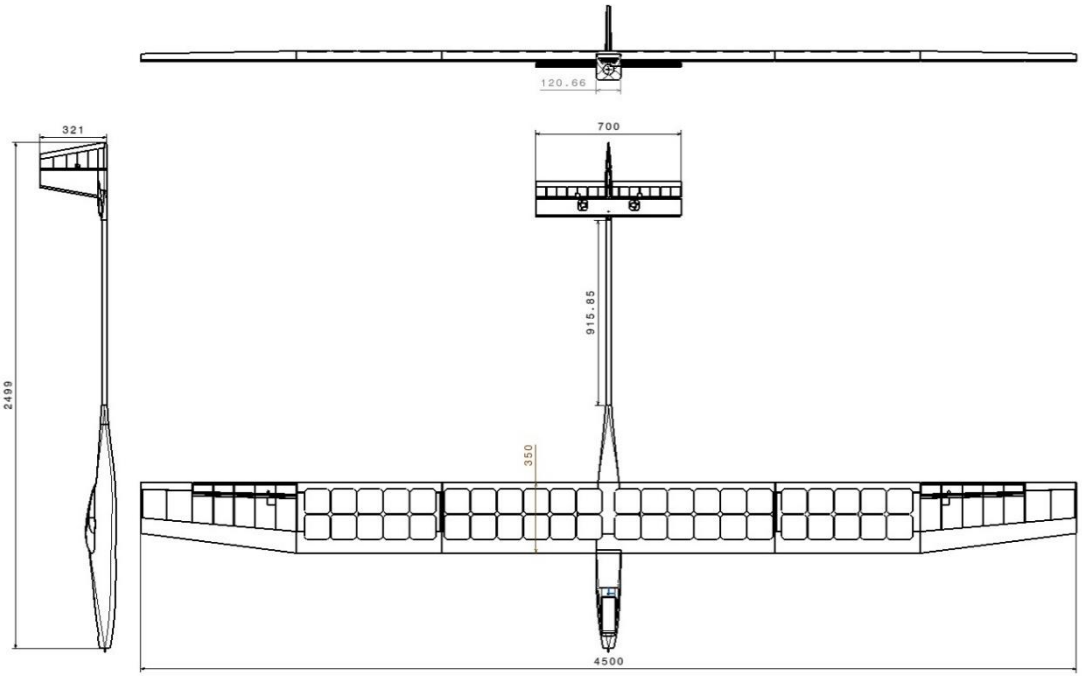

Figure 2.11 - CAD 3-views of the LEEUAV.

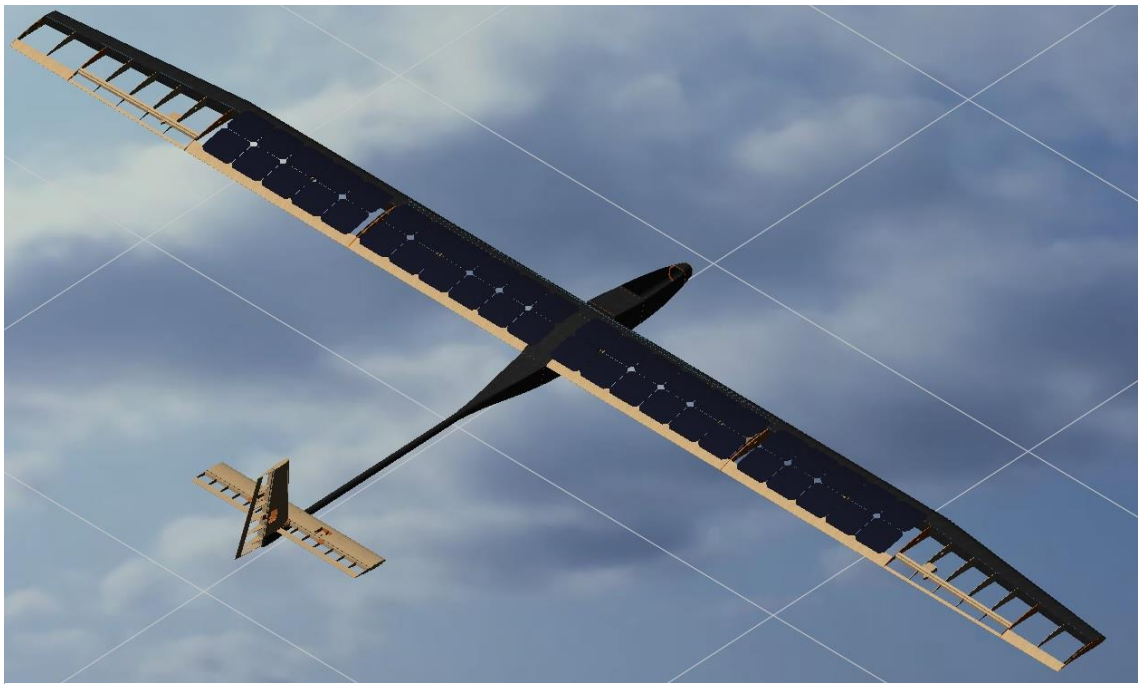

Figure 2.10 - LEEUAV airframe.

Chapter 3: Structure of the LEEUAV

3.1 Material Selection

The material selected to fabricate the UAV is essential as this will determinate the success or failure of the whole project. The structure of UAV must be lightly but stronger to withstand all forces acting on it.

The most common material used in UAV is the wood and composites.

3.1.1 Composites

This project used the bidirectional (0º and 90º) carbon fibre due the high strength in both directions, vertical and horizontal. This material has also good labour using the lay-up in complex geometry like in this structure. The properties of this material can be seen on Table 3.1. This project has two carbon fibres: the $90\ g/m^2$ and the $190\ g/m^2$.

Table 3.1 – High strength Carbon-Epoxy specifications

	Unit	Value
Longitudinal Young's Modulus	$[Pa]$	$3.50 * 10^{10}$
Transverse Young's Modulus	$[Pa]$	$3.50 * 10^{10}$
In-plane shear Modulus	$[Pa]$	$2.50 * 10^{9}$
Major Poisson ratio	$[-]$	0.1
Ultimate longitudinal tensile strength	$[Pa]$	$3.00 * 10^{8}$
Ultimate longitudinal compressive strength	$[Pa]$	$2.85 * 10^{8}$
Ultimate transverse tensile strength	$[Pa]$	$3.00 * 10^{8}$
Ultimate transverse compressive strength	$[Pa]$	$2.85 * 10^{8}$
Ultimate in-plane shear strength	$[Pa]$	$4.50 * 10^{7}$
Density	$[Kg/m^3]$	1600

3.1.2 Wood

The wood was chosen to the internal structure which has as properties a low density and a good hand labor comparing with other materials. The most utilized woods are the balsa and birch plywood which are often used for different applications. The Table 3.2 compares the properties of this two materials.

Table 3.2 - Wood average properties[19]

Properties	**Balsa**	**Birch Plywood**
Density $[Kg/m^3]$	130	700
Elastic Modulus $[GPa]$	3	18
Shear Modulus $[GPa]$	0.23	1.3
Tensile Strength: Ultimate $[MPa]$	14	40

The previous table conclude that the balsa is lighter and cheaper than the birch plywood and is easier to trim so it can be applied on the internal structure of the horizontal and vertical tail. On other hand the birch plywood is more strength and is light as well, so it is applied if reinforcements needed.

3.2 Design

3.2.1 Horizontal tail

The horizontal tail uses a symmetrical aerofoil, NACA0010, with $700\ mm$ span and 175 mm chord and it are divided in a fix and a flexible structure.

The fix structure is a rigid structure with $700\ mm$ span and $180\ mm$ chord. It is composed by a leading edge, a spar, ribs and skin. The leading edge is a balsa sheet 8.5 mm high. The ribs provide the aerofoil shape and it was made using a 1.6mm thick balsa wood, except on the connection structure, explained later. The ribs were placed equidistant along the span with a total of 16 ribs. The spar is the principal structure of the fix structure which carries the bending moment. It is composed by a sheet of balsa with 6mm width but due the low balsa strength, two carbon fibre strip were added on each edge of the sheet with $0.6\ mm$ of thick. The skin covers the internal structure with a 1.6mm thick balsa wood and also provides the load transfer into the ribs and the spar.

The servos were attached to the fix structure using an appropriate structure. This structure needs to be strong enough to withstand the load from the control-servos. It is composed by two ribs and two stringers with 1.6mm thick balsa wood reinforced with 1mm thick birch plywood. It has $50\ mm$ width and $50\ mm$ length. The servo is connected to the stringers by two screws with $1\ mm$ radius. The servo controls the flexible structure using a servo-arm attached to a

horn. The horn is attached on the flexible structure using a square with 2mm thick birch plywood.

The flexible structure or elevator is a light structure divided in two with 335mm span each and it's connected to the fix structure using three 3 hinges. It is composed by a leading edge, ribs and a trailing edge. The leading edge has a triangle configuration to be able the movement and it's made by balsa with 10mm thick. The ribs provide the aerofoil shape and it is composed by 8 ribs, in each elevator, using a 1.6mm thick balsa wood. It was designed with the same profile as the aerofoil but next to the trailing edge. It was designed two slots to place the trailing edge. Due to this change the trailing edge was composed by two sheets of balsa with 1.6 thick, each.

The Figure 3.1 shows the internal structure of the horizontal tail.

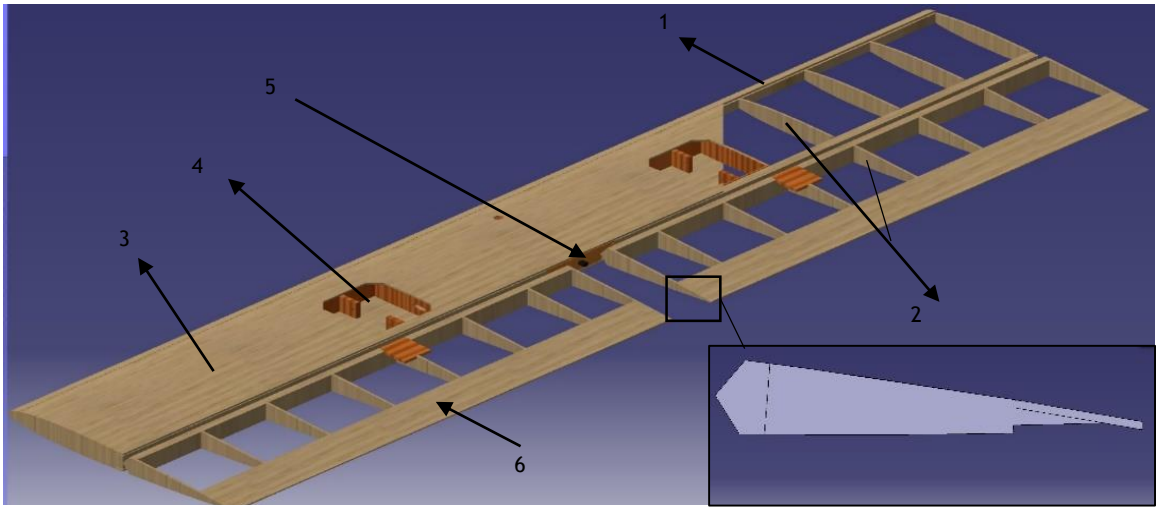

Figure 3.1 – Horizontal stabilizer structure (1-Leading edge; 2-Ribs; 3-Skin; 4-Servo Structure; 5-Spar; 6-Trailling edge).

The horizontal tail needs to be removed from the empennage support due to the mission requirements. The best solution was to use two carbon fibre rod, attached to the main spar, to prevent the horizontal tail to roll and use a screw, near the leading edge, to position. This option needed some changes on internal structure due to the low strength of the balsa. So to the main spar was added a chamfer of 6mm thick birch plywood to position the carbon fibre rod and on the leading edge a sheet with two ribs in each side with $30x30x3\ mm$. The Figure 3.2 shows in detail the connection structure.

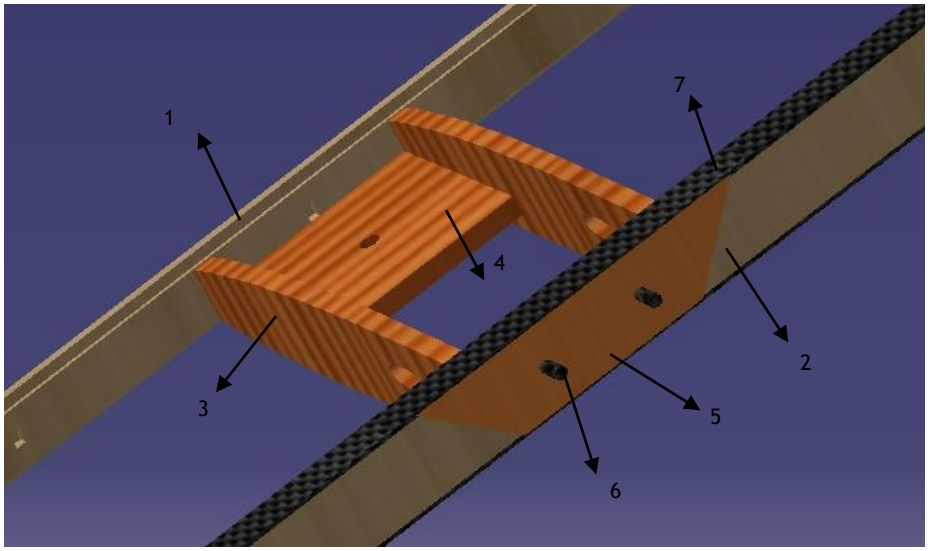

Figure 3.2 - Connection structure (1-Leading edge; 2-Spar; 3-Rib; 4-Screw reinforcement; 5-Spar reinforcement; 6-Carbon fibre rod; 7-Carbon fibre strip).

3.2.2 Vertical tail

The vertical stabilizer uses a symmetrical aerofoil, NACA 0010 and it composed by a fix and flexible structure.

The fix structure is a rigid structure with $280\,mm$ span and $85\,/\,140\,mm$ tip and root chord, respectively. The internal structure has the same function as on the horizontal tail. The leading edge is a sheet of balsa with the same profile as the aerofoil. The ribs were placed equidistant along the tail span using a 1.6 mm thick balsa wood. The spar had two carbon fibre strip on each edge of the 6 mm thick balsa wood. The spar was extended to be able to connect the elevator with three hinges. Finally the skin is a 1.6 mm thick balsa wood that covers all the internal structure. The servo is placed on a servo structure using two ribs and two stringers with 1.6 mm of balsa reinforced with 1 mm thick of plywood.

The vertical tail servo was placed with the same objective explained previously. It is composed by two ribs and two stringers with $1.6\,mm$ thick balsa and reinforced by $1\,mm$ thick birch plywood. It has three sheets of plywood with $2\,mm$ to connect the servo.

The flexible structure or rudder has the same configuration as the elevator with a 320 mm span and 85/140 tip and root chord, respectively.

The Figure 3.3 shows the internal configuration of the vertical tail as well the servo structure.

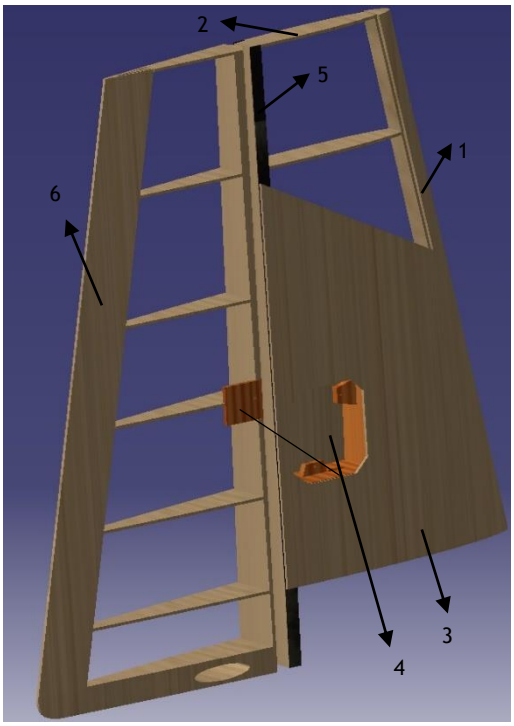

Figure 3.3 –Vertical stabilizer structure (1-Leading edge; 2 -Rib; 3-Skin; 4-Servo Structure; 5-Spar; 6-Trailling edge).

3.2.3 Fuselage

The fuselage is the principal structure of the LEEUAV that carries all the components needed to perform the mission and where the structures, like the wing and tail tube, are connected.

This structure is made by carbon fibre with frames and longerons to increase the stiffness. It has $1.20\,m$ length with $0.121\ m$ and $0.124\ m$ maximum width and height, respectively. The access to the interior of the fuselage was made by adding two access hatches on the front and the back of the fuselage. The front access hatch, which objective is to access the motor and it is covered by a carbon fibre structure. The other access hatch is placed between the two connections points of the wing.

The internal structure, as well as, the connection structure with the wing and tail tube, are explained in the next sub-chapters.

3.2.3.1 Internal Structure

The internal structure is placed to reinforce the skin by taking some of the bending stress from the fuselage structure. It is built using birch plywood with different thickness and it is composed by six frames, two stringers and one screw reinforcement. The Figure 3.4 shows the internal structure position.

The motor frame with 4mm thick was placed in the front of the fuselage to attach the motor. The two cover frames were attached due to the access hatch, both have a 2mm thick.

The fuselage tube and the tube frame were placed on the back of the fuselage due the connection with the tail tube, explained in the next sub-chapter. The fuselage tube is a Woven finish carbon fibre[1] with an outside diameter of 27 mm and an inside diameter of 25mm and the frame tube has 4 mm thick.

The leading edge frame was placed to attach the two carbon fibre rods of the wing and it was used a $4\,mm$ thick birch plywood.

Regarding the two screws, it was placed two stringers between each frame to place the screw reinforcement and to transfer the weight and the aerodynamic forces to the leading edge frame and the trailing edge frame.

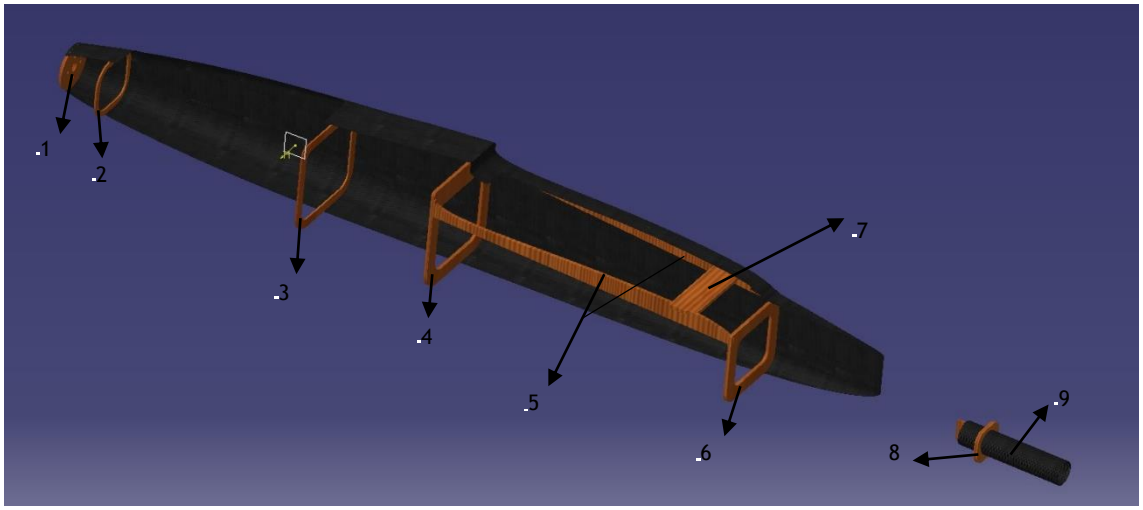

Figure 3.4 - Fuselage internal structure (1-Motor frame; 2-Cover frame; 3-Cover frame; 4-LE frame; 5-Stringers; 6-TE frame; 7-Wing screws reinforcement; 8-Frame tube; 9-Fuselage tube).

3.2.3.2 Connection Structure

The connection structure between the tail tube and the fuselage has to be stiff to transfer the weight and the aerodynamic forces into the fuselage. This structure needs to support the rotation, as well as, the motion of the tail tube. The best solution was to use a cross and a screw.

The cross has the objective to support the rotation of the tail tube. It is made using a 2 mm thick of birch plywood attached into the fuselage tube with the same width as the tube radios and with 3 cm of length. On the tail tube two light cuts with the same width and length of the cross were made. The screw is placed near the datum of the fuselage to stop the tube motion. This structure is shown in the Figure 3.5.

[1] Woven Finish tube is manufactured from alternating layers of unidirectional prepreg carbon fibre for a maximum strength.

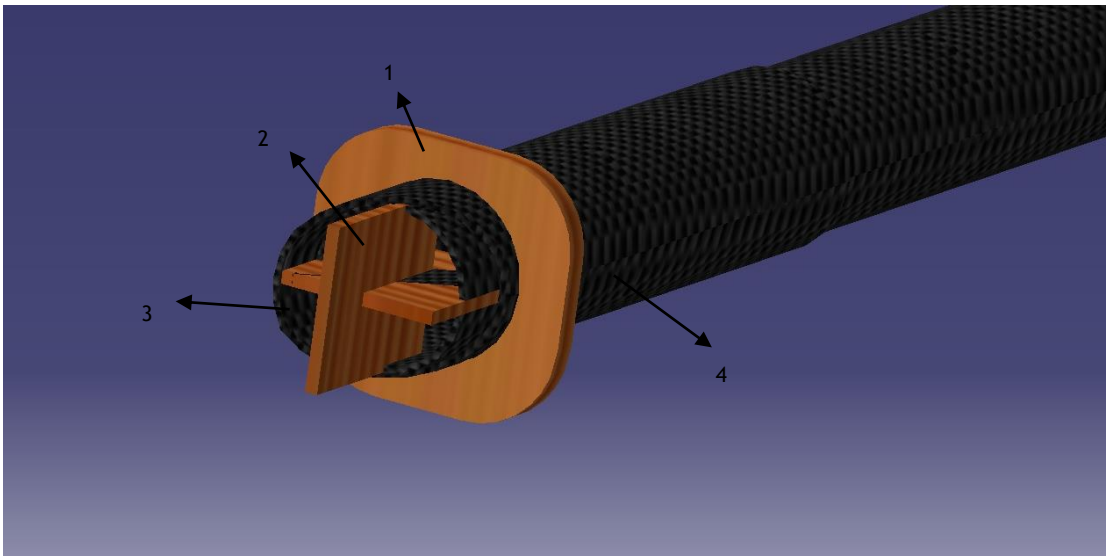

Figure 3.5 - Connection Fuselage-Tail tube (1-tube frame; 2-cross; 3-tail tube; 4-fuselage tube).

The fuselage structure as well as the internal structure are analyzed using the finite element model on the sub-chapter 3.5.

3.2.4 Tail tube

The tail tube is a Woven Finish Carbon Fibre with an 1005 mm length, $23/25$ mm diameter (interior/exterior).

The tail tube connects the empennage support to the fuselage. The empennage support is glued into the fuselage. On the other hand, the tail tube is connected to the fuselage using a cross and a screw, as explained previous.

During the fabrication it's essential to be very careful, while placing the fuselage tube, as it will be the reference to the tail tube.

3.2.5 Tail Support

The tail support, as its named, it is where both tails will be connected. This structure consists on a carbon fibre structure, with 246 mm length. It has the aerofoil profile for the horizontal tail with the -3 angle of attack and a flat surface to attach the vertical tail. The internal structure is composed by two frames and one aerofoil frame with 2 mm thick of birch plywood, Figure 3.6. The aerofoil frame is placed along the empennage support to attach the vertical tail. The two frames (first and second frame) are placed to positioned and transfer the load from the aerofoil frame into the structure. The first frame also helps the connection of the horizontal tail.

This structure is analysed on the 3.4 sub-chapter.

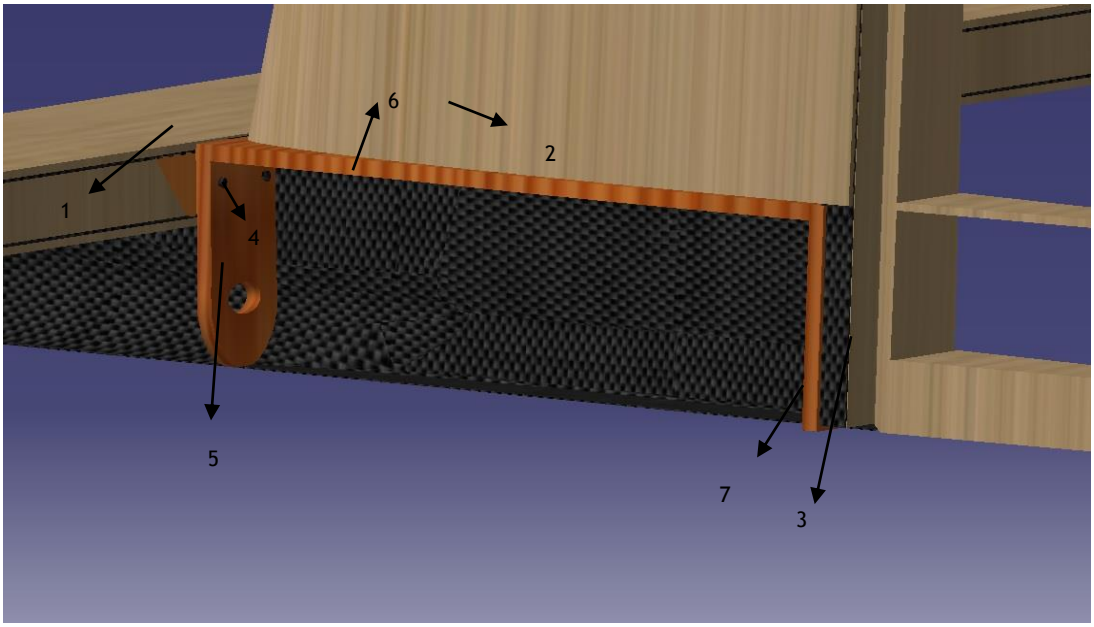

Figure 3.6 – Empennage support structure. (1-Horizontal tail spar;2-Vertical tail;3-Vertical tail spar;4-Carbon rod;5-First frame;6-Aerofoil frame;7-Second frame).

3.3 Loads

Before the structure is sized and analyzed using a primarily sizing and the FEM model, the loads that will sustain must be determined, as this will define the efforts and moments that the structure can support.

For that, the loads determined were the shear force, inertia, the maneuvering, the gust and the balancing loads using the CS-VLA[16].

First of all was determined the positions of all components needed to perform the mission, like the payload and the battery. It was used the relative position of the CG where it must be between $25\% - 30\%$ of the root chord. The CG was determined following the next steps: determine the weights and arms of all mass within the UAV; multiply weights by arms of all mass to calculate moments; add the moments of all mass together; and dividing the total moment by the total weight of the aircraft give us an overall arm of the CG. The dimensions were measured by using the *measure inertia* tool from CATIA®.

Where:

$$\sum W = 49.318\ [K_g] \text{ and } \sum M = 27.754\ [N.m] \qquad 3.1$$

Dividing, the Center of gravity become:

$$CG = \frac{\sum M}{\sum W} = 0.563\ [m] \qquad 3.2$$

So the percentage of CG:

$$\%CG = \frac{CG - \overline{LE}}{C_r} * 100 = 25\% \quad 3.3$$

The Table 3.3 shows the results of the components location.

Table 3.3 - Components location

Components	Weight $[N]$	CG component $[m]$	Moment $[N.m]$
Motor frame	0.039	0.001	$5.101E-05$
Motor	1.938	0.026	0.050
cover frame1	0.020	0.051	0.001
Battery	7.358	0.126	0.925
cover frame2	0.049	0.309	0.015
LE frame	0.168	0.468	0.079
Payload	15.696	0.500	7.848
Wing	15.706	0.603	9.469
solar panel	5.100	0.613	3.126
TE frame	0.110	0.821	0.090
Tube frame	0.010	1.101	0.011
Fuselage tube	0.154	1.250	0.193
Tail tube	1.197	1.618	1.937
EH	1.048	2.204	2.309
1 frame	0.029	2.223	0.065
Aerofoil frame	0.059	2.289	0.135
Empennage Support	0.137	2.307	0.317
EV	0.589	2.352	1.384
2 frame	0.020	2.355	0.046

3.3.1 Shear force

The force applied on the structure can cause normal stress, being either tension and compression stress or shear stress and bending moment which cause normal stress. These analysis studies the shear force and the bending moment present on the structure.

After determine the shear force and the bending moment was assumed a beam in a static equilibrium to find the lift from both tails. So using the principle of virtual forces a beam in static equilibrium state the net force and net torque acted upon the system is zero, Eq.(3.4) and Eq.(3.5).

$$\sum \vec{F} = 0 \quad (3.4)$$

$$\sum \vec{M} = 0 \quad (3.5)$$

Replacing the summation of the force to the summation of the weights plus the load factor and the lift force from the wing $(L_W)$and also the horizontal stabilizer (L_H), Eq.(3.6).Likewise, replacing the summation of the moment to the summation of weights plus the distance and the lift force from the wing and horizontal stabilizer plus the distance to a reference point, Eq. (3.7), the reference used was the datum in the front of the fuselage.

$$\sum nW_i + L_W + L_H = 0 \tag{3.6}$$

$$\sum nW_i x_i + x_W L_W + x_H L_H = 0 \tag{3.7}$$

These two equations have two variables so its needs to solve the system in order to (L_W) and (L_H),Eq.(3.8) and Eq.(3.9):

$$L_W = -L_H - \sum nW_i \; i = 1,2,3 \ldots \tag{3.8}$$

And:

$$L_H = \frac{x_w \sum nW_i - \sum nW_i x_i}{x_H - x_w} \; i = 1,2,3 \ldots \tag{3.9}$$

So the shear force is, Eq.(3.10):

$$F_i = \sum_{i=1}^{j} F_{i-1} n \;, j = 1,2,3 \ldots \tag{3.10}$$

And the bending moment, Eq.(3.11):

$$M_i = \sum_{i=1}^{j} F_{i-1}(x_i - x_{(i-1)}) n \;, j = 1,2,3 \ldots \tag{3.11}$$

The Figure 3.7 and Figure 3.8 shows the shear force and bending moment, respectively, on the structure with an $5cm$ interval [1].

[1] The results for each point is on Table A.1.

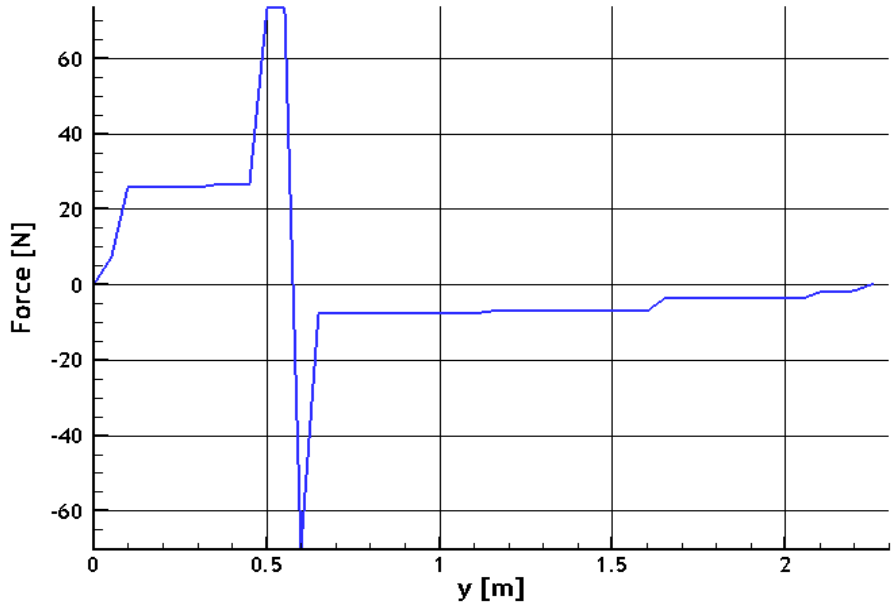

Figure 3.7 – Shear force versus fuselage length.

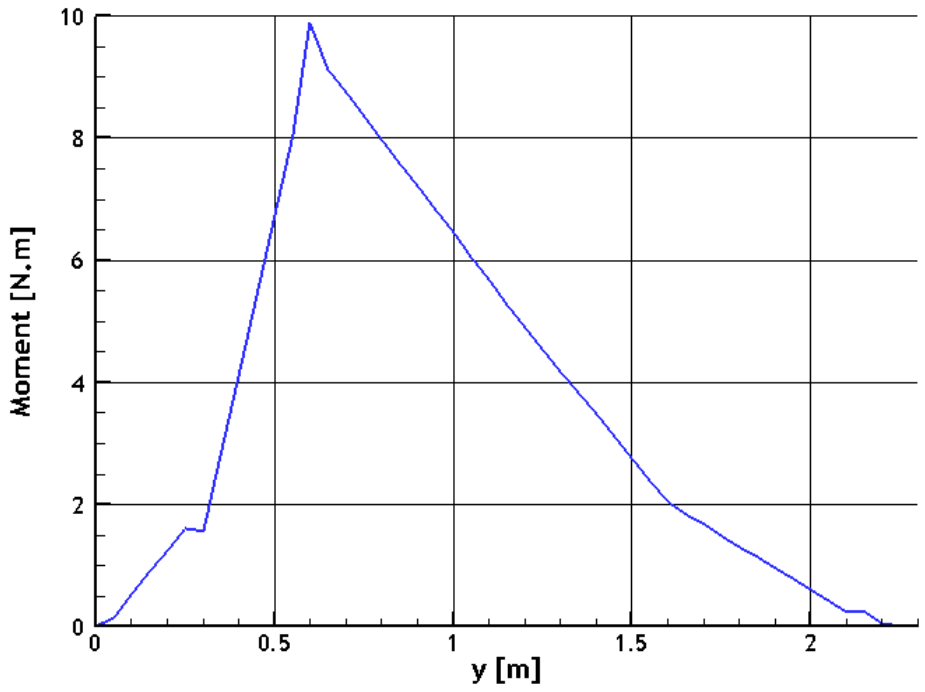

Figure 3.8 – Bending moment versus fuselage length.

3.3.2 Inertia Loads

The inertia loads refer to the objects that experiences in the aircraft a force equal to object's weight times the aircraft load factor. This creates stresses throughout the aircraft that must be determined.

After knowing the right positions of all components, the inertial load can now be determined by the weight of the components times the aircraft factor, Table 3.4.

Table 3.4 - Inertia Loads

Components	Inertia loads [N]
Firewall frame	0.118
Motor	5.815
Cover frame1	0.059
Battery	22.073
Cover frame2	0.147
LE frame	0.503
Payload	47.088
Wing	47.117
Solar Panels	15.301
TE frame	0.330
Tube frame	0.029
Tube	0.462
Tail tube	3.590
Horizontal tail	3.144
1 frame	0.088
Aerofoil frame	0.177
Empennage Support	0.412
Vertical tail	1.766
2 frame	0.059

3.3.3 Horizontal tail Loads

The loads in the horizontal tail can be considered one of the most important aspects of a structural analysis, as they affect parts of the structure, like the rear and the center section of the fuselage.

For this reason, it is necessary to determine the manoeuvring, the balancing, and the gust loads.

Table 3.5 - Horizontal tail dimensions[9]

Dimension			
Lift slope	a_{ht}	$[1/rad]$	4.66
Area	S_{ht}	$[m^2]$	0.123
Downwash factor	$\left(1-\frac{d\varepsilon}{d\alpha}\right)$	$[-]$	0.777
Tail arm	l_{EH}	$[m]$	1.584

3.3.3.1 Balancing Loads

The horizontal tail balancing load is a load necessary to maintain equilibrium in any specified flight condition with no pitching acceleration. Using the CS-VLA it was determined using two load factors: n=1 and n=n_{max}.

The balancing load is determined using the equilibrium of all weights in the maximum speed:

$$\sum \vec{F} = 0 \tag{3.12}$$

$$\sum \vec{M} = 0 \tag{3.13}$$

Replacing the forces and the moments using the Table 3.4:

$$\sum nW_i + L_W + L_{H_B} = 0 \tag{3.14}$$

$$\sum nW_i x_i + x_W L_W + M_0 + x_H L_{H_B} = 0 \tag{3.15}$$

The balancing load from the horizontal tail to the maximum load factor became:

$$L_{H_B} = -14.54 \text{ N} \tag{3.16}$$

And to the minimum load factor:

$$L_{H_B} = -13.45 \text{ N} \tag{3.17}$$

3.3.3.2 Maneuver Loads

The horizontal tail can be imposed by the manoeuvring loads during the flight and it is an increment to the balancing loads. This is determined using the two conditions present on the CS-VLA.

The horizontal tail load increment is:

$$L_{EH_M} = \ddot{\theta}\frac{WK_y^2}{g l_{EH}} \tag{3.18}$$

Where to a down load (n=1) the angular acceleration is:

$$\ddot{\theta} = 20 n_{max} \frac{n_{max} - 1.5}{V} \tag{3.19}$$

And to an up load (n=n_{max}):

$$\ddot{\theta} = -20 n_{max} \frac{n_{max} - 1.5}{V} \tag{3.20}$$

The radius of gyration in meters is the square root of the Inertia moment dividing by the total mass in Kg.

$$K_y = \sqrt{\frac{I_{yy}}{m}} \tag{3.21}$$

The moment of inertia the summation of the max plus the distance in relation to CA of the wing.

$$I_{yy} = \sum m_i (x^2 + z^2) \quad i = 1,2,3, \dots \tag{3.22}$$

For the n=n_{max} the horizontal load increment was:

$$L_{EH_M} = -20.063\ N \tag{3.23}$$

For the n=1:

$$L_{EH_M} = 6.68\ N \tag{3.24}$$

3.3.3.3 Gust Loads

Gust loads are an increment to the balancing loads, resulting of wind gusts that could happen during the flight.

The increment is:

$$L_{EH_G} = \frac{K_g U_{de} V a_{ht} S_{ht}}{16.3} \left(1 - \frac{d\varepsilon}{d\alpha}\right) \tag{3.25}$$

The gust alleviation factor is defined:

$$K_g = \frac{0.88 \mu_g}{5.3 + \mu_g} \tag{3.26}$$

And the aeroplane mass ratio:

$$\mu_g = \frac{2 * \left(\frac{m}{S}\right)}{\rho \bar{c} a} \tag{3.27}$$

The increment of the gust load is determined to the negative and the positive derived gust velocity U_{de}, which is $15.24\ m/s$ to the cruise speed and 7.62 to the design dive speed. So the increment of the gust loads results, Table 3.6.

Table 3.6 - Gust loads

Increment of the gust load	Units $[N]$
$\boldsymbol{U_{de} = 15.24\ \mathbf{m/s}}$	3.446
$\boldsymbol{U_{de} = 7.62\ \mathbf{m/s}}$	4.485
$\boldsymbol{U_{de} = -15.24\ \mathbf{m/s}}$	−3.446
$\boldsymbol{U_{de} = -7.62\ \mathbf{m/s}}$	−4.485

The horizontal tail loads can be resume in the follow Table 3.7. It was sum the maximum value of the balancing load with the maximum increment of both maneuver and gust loads and it was sum the minimum value of the balancing load with the minimum increment of both maneuver and gust loads. As the gust loads had four results it was sum the maximum and minimum of the positive derived gust speed and for the negative derived gust speed was made the same.

Table 3.7 - Horizontal tail loads

	Horizontal tail Load	Value $[N]$
1	L_{H_B} maximum	-13.45
2	L_{H_B} minimum	-14.54
3	$L_{H_B} + L_{EH_M}$ maximum	-34.60
4	$L_{H_B} + L_{EH_M}$ minimum	-6.76
5	$L_{H_B} + L_{EH_G} \rightarrow U_{de}\ positive$ maximum	-8.96
6	$L_{H_B} + L_{EH_G} \rightarrow U_{de}\ positive$ minimum	-11.09
7	$L_{H_B} + L_{EH_G} \rightarrow U_{de}\ negative$ maximum	-16.89
8	$L_{H_B} + L_{EH_G} \rightarrow U_{de}\ negative$ minimum	-19.02

3.3.4 Vertical tail Loads

The loads in the vertical tail affect other parts of the structure, like the rear and the center section of the fuselage. For that, only the manoeuvring and the gust loads are considered and they were determined using the CS-VLA.

The Table 3.8 give a sum of the Vertical Stabilizer dimensions.

Table 3.8 - Vertical Stabilizer dimensions[9]

Dimension		Units	Value
Aerodynamic centre position	Z_{ca}	$[m]$	0.140
Area	S_v	$[m^2]$	0.065
Aspect Ratio	AR_v	$[-]$	1.364
Chord	c	$[m]$	0.218
Distance from aeroplane CG to lift centre o fvertical surface	$Z_{ca}l_v$	$[m]$	1.734
Lift slope	$\frac{dC_l}{d\beta}$	$[1/rad]$	2.443
Rudder chord	c_f	$[m]$	0.114
Span	b	$[m]$	0.297

3.3.4.1 Maneuver Loads

The vertical stabilizer produces a lateral force, Figure 3.9, due to the lateral lift applied on the aerodynamic centre and it is denoted by, L_v. This force transmits to the fuselage a yawing moment.

This force can be obtained by the vertical tail lift coefficient, the velocity and the tail area, Eq.(3.28)[16].

$$L_v = \frac{1}{2}\rho V^2 S_V C_{L_V} \tag{3.28}$$

The vertical tail lift coefficient is the sum of the vertical tail lift curve slope a_{1V}, and rudder "lift curve slope" a_{2V}.

$$C_{L_V} = a_{1V}\beta + a_{2V}\delta_V \tag{3.29}$$

Where:

$$a_{1V} = \frac{dC_L}{d\beta} = \frac{\frac{dc_l}{d\beta}}{1 + \frac{dc_l}{d\beta}\frac{(1+\tau)}{\pi A}} \tag{3.30}$$

And:

$$a_{2V} = \frac{dC_L}{d\delta} \approx \sqrt{\frac{c_f}{c}}\frac{dC_L}{d\beta} \tag{3.31}$$

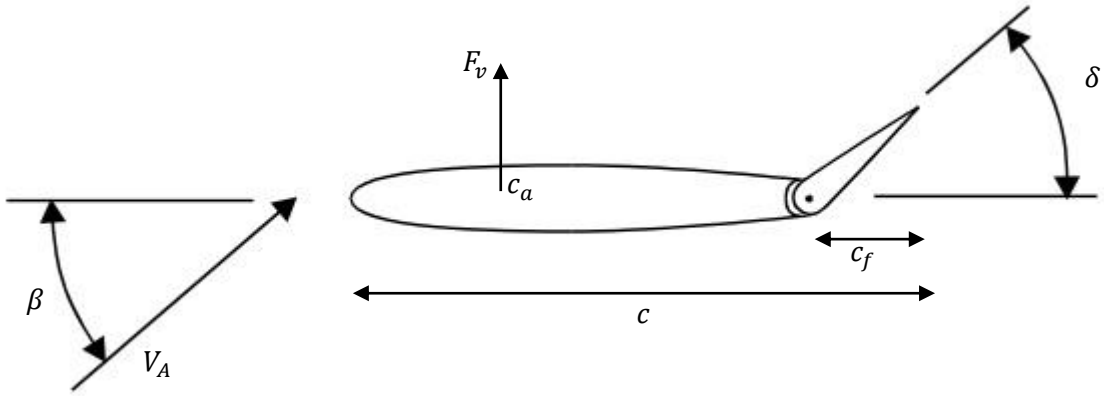

Figure 3.9 – Vertical Stabilizer components.

Replacing the Eq.(3.29) on Eq.(3.28):

$$L_v = \frac{1}{2}\rho V^2 S_V (a_{1V}\beta + a_{2V}\delta_V) \tag{3.32}$$

The force is calculated to three different stages to find the maximum force applied:

1. $V = V_A \qquad \delta_V = \delta_{max} \qquad \beta = 0°;$
2. $V = V_A \qquad \delta_V = -\delta_{max} \qquad \beta = 15°;$
3. $V = V_A \qquad \delta_V = 0 \qquad \beta = 15°;$

Where it differs on the maximum and minimum deflection (δ_V), the yaw angle (β) and the velocity (V). The deflection maximum is $30°$ and the velocity is the cruise speed. The Table 3.9 shows the calculus of the vertical tail lift curve, the rudder "lift curve slope" and the vertical force.

Table 3.9 - Vertical Tail Force

Stage/Force	**1**	**2**	**3**
$\boldsymbol{a_{1V}}$	1.555272	1.555272	1.555272
$\boldsymbol{a_{2V}}$	1.122749	1.122749	1.122749
$\boldsymbol{L_v}$	14.57	−64.79	10.09

3.3.4.2 Gust Loads

The gust loads from the CS-VLA are 7.5m/s to dive velocity and 15m/s to cruise speed.

The gust load of vertical tail can be determined as follows:

$$L_{vt} = \frac{K_{gt} U_{de} V a_{vt} S_{vt}}{16.3} \tag{3.33}$$

Where the gust alleviation factor is:

$$K_{gt} = \frac{0.88\mu_{gt}}{5.3 + \mu_{gt}} \tag{3.34}$$

And the lateral mass ratio:

$$\mu_{gt} = \frac{2M}{\rho \bar{C}_t g a_{vt} S_{vt}} \frac{2m}{\rho \bar{C}_t g a_{vt} S_{vt}} \left(\frac{K_z}{l_v}\right) \tag{3.35}$$

The radius of gyration in yaw is the summation of the mass plus the distance to the wing CA.

$$K_z = \sum m_i (x^2 + y^2) \tag{3.36}$$

These loads are applied on the aerodynamic centre of the vertical tail and are transmitted to the fuselage by a yaw moment.

$$T = L_v z_{ca} \tag{3.37}$$

3.4 Preliminary sizing

The preliminary analysis had the objective to give a first sizing of the structure and also to define the critical areas.

The preliminary sizing used a spreadsheet to determine the shear and normal stress present on the aircraft.

3.4.1 Shear flow

Knowing the shear force, determined previously, the shear flow is, Eq.(3.38):[17].

$$q_s = \left(\frac{S_x I_{xx} - S_y I_{xy}}{I_{xx} I_{yy} - I_{xy}^2}\right) \int_0^s t x ds - \left(\frac{S_y I_{yy} - S_x I_{xy}}{I_{xx} I_{yy} - I_{xy}^2}\right) \int_0^s t x ds \tag{3.38}$$

As the fuselage is symmetric and the only shear force is on axis x, the $I_{xy} = 0$ and $S_x = 0$, so it becomes:

$$q_s = -\left(\frac{S_y}{I_{xx}}\right) \int_0^s t x ds \tag{3.39}$$

Where:

$$I_{xx} = \int y^2 dA \tag{3.40}$$

It was assumed a generic quadratic cross section, Figure 3.10, with the follow second moment of area, Eq.(3.12). The dimensions to each section was determinate by using the measure tools of CATIA®;

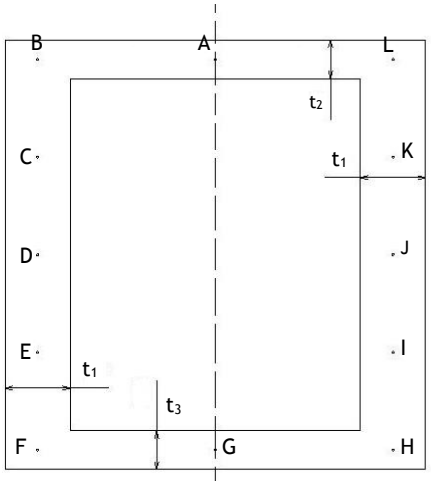

Figure 3.10 – Fuselage quadratic section.

$$I_{xx} = \frac{1}{12}Lh^3 - \frac{1}{12}(L - 2t_1)[h - (t_2 - t_3]^3 \tag{3.41}$$

The bending moment cause the normal stress and is determinate by the Eq.(3.42).

$$\sigma_z = \left(\frac{M_y I_{xx} - M_x I_{xy}}{I_{xx} I_{yy} - I_{xy}^2}\right)x + \left(\frac{M_x I_{yy} - M_y I_{xy}}{I_{xx} I_{yy} - I_{xy}^2}\right)y \tag{3.42}$$

$$\sigma_z = \frac{M_x * y}{I_{xx}} \tag{3.43}$$

Computing for each point, represent on Figure 3.10, and for each section, the results can be seen on Appendix A.2.

3.4.2 Results

The objective for this analysis, is to predict the value of carbon thickness, so it needs to compare the values of shear force and normal stress to the admissible normal and shear strength. The admissible strength Table 3.10 is the reference values of the carbon fibre dividing by two factors; the quality factor and security factor. These factors can be different for each application/structure, in this structure the values used were $1.5/1.1$ to security factor and quality factor, respectively.

Table 3.10 – Reference values of strength

	Unit	Value
Admissible tensile strength	[Pa]	$2.12 * 10^{10}$
Admissible compressive strength	[Pa]	$2.12 * 10^{10}$
Admissible shear strength	[Pa]	$1.52 * 10^{9}$

Comparing the admissible strength with the shear stress and normal stress determinated previous, the values can be:

1. $\frac{\sigma_1}{\sigma_{adm}} < 1$ and $\frac{\tau_1}{\tau_{adm}} < 1$ These values show that the normal and shear stress are below the admissible strength, which indicates that the structure is secure;
2. $\frac{\sigma_1}{\sigma_{adm}} = 1$ and $\frac{\tau_1}{\tau_{adm}} = 1$ These values show that the normal and shear stress are equal which indicates that the structure is not safe.
3. $\frac{\sigma_1}{\sigma_{adm}} > 1$ and $\frac{\tau_1}{\tau_{adm}} > 1$ These values show that the normal and shear stress are higher than the admissible strength, which indicates that the structure is critical.

Computing and having in consideration the previous reference, the results of the preliminary sizing show that the fuselage with a thickness of $0.4\,mm$ have a ratio under 1. But on the connection to the tail, the shear force increases to values that the ratio is over 1 which indicates that the fuselage can failure. In order to low the shear stress, the thickness of carbon fibre had to be increased till $0.94\,mm$. This value of thickness was added on the last $10\,cm$ of the fuselage. These results can be seen on Table A.2, Table A.3.

Regarding the empennage support the structure is secure to a value of $0.24\,mm$ of thickness. Comparing the values obtained, Table A.5 and Table A.4, the conclusions is that both, normal and shear stress, are bellow to the admissible strength.

3.5 Finite Element Model

For finite element analysis of the LEEUAV structure the ANSYS® Mechanical software[18] was used. This program uses the finite element analysis tool for structural analysis, including linear, nonlinear and dynamic studies. This simulation product provides a complete set of elements behaviour, material models and equation solvers for a wide range of mechanical design problems.

The ANSYS® have a series of models that can be chosen depending on the necessity of the simulation. For this analysis the model used was the Static Structural and the components analyse was the fuselage with the tail tube. The fuselage has the nominal thickness of $4\,mm$ and on the datum of the fuselage a $9.4\,mm$ thickness as result of the preliminary sizing.

The first step was to upload the STP file into the ANSYS® is to upload the file using the STP format.

The mechanical properties of the materials were insert using both the orthotropic properties defined on Table 3.1 and Table 3.11.

Table 3.11 – Mechanical properties of plywood[19]

	Value	Value
Density	$[Kg/m^3]$	410
Young modulus X direction	$[MPa]$	8556
Young modulus Y direction	$[MPa]$	3444
Young modulus Z direction	$[MPa]$	3444
Shear modulus XY direction	$[MPa]$	71
Shear modulus YZ direction	$[MPa]$	25
Shear modulus XZ direction	$[MPa]$	25

3.5.1 Generation of the Numerical Mesh

The next step it's the most important aspect to any structure analysis using the ANSYS®, is the generation of model mesh. The aim of this mesh is to provide a smoot distribution of points where the solution will be calculated, and the finer the grid better will be the results. But it's necessary to take under consideration that, a finer grid has, as consequence, an increase on computational cost (CPU).

After generate the numerical mesh it was inserted the connection points using the automatic method on ANSYS®, except on the connection between the fuselage and tail tube. In this connection it was inserted manually the contact between the fuselage tube-fuselage; and the tail tube-fuselage tube.

The generation of the numerical mesh can influence the results of the solution so a convergence analysis of the finite element model was carried out to assess the sensitivity of the maximum tube deflection as a function of the number of elements in the grid. This study considered a fix contact between the fuselage and the wing. The refinement of the grid mesh was done by changing the element size to $5x10^{-3}\ m$ and by using the features of the mesh refinement and body sizing. The figure x shows the convergence of the number of elements for the maximum tail deflection. It's possible to conclude that the solution stabilizes around 980000 elements but for computational reasons the number of elements used was 948211 elements[1] which has a relative difference of 0.84 %.

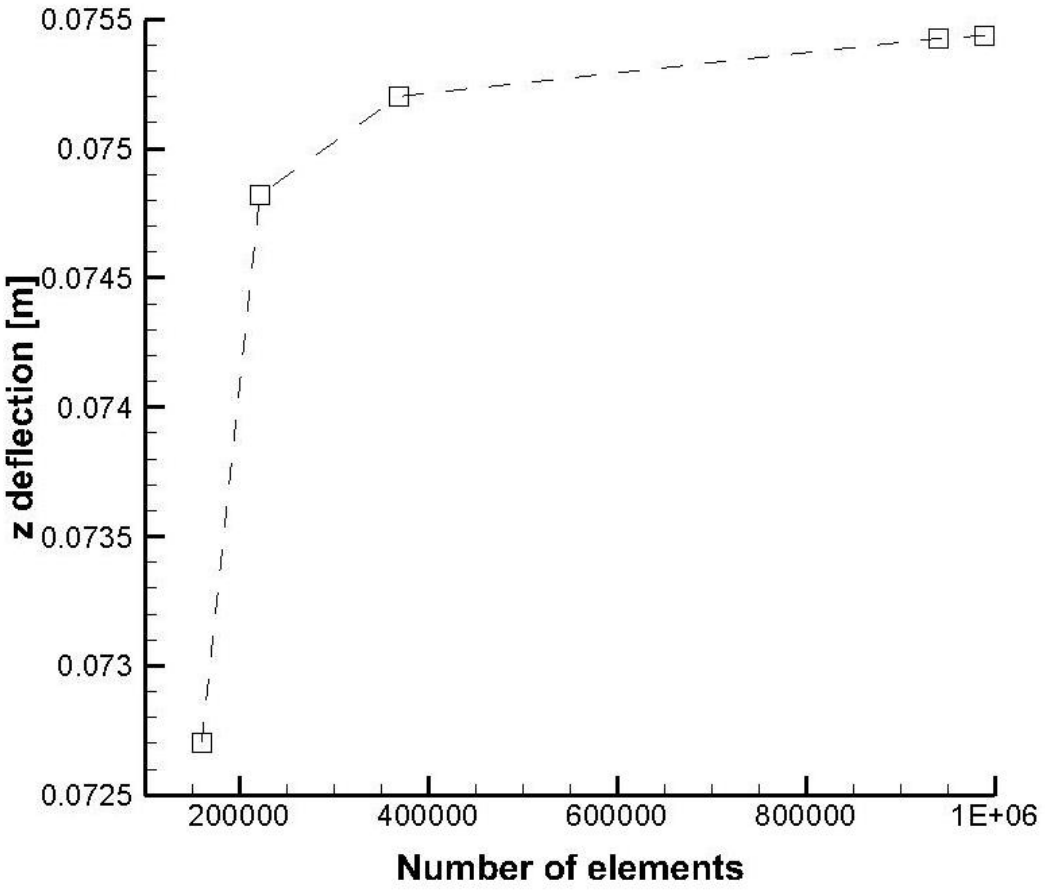

The mesh type was changed according to the geometry. The tube, the frames and the fuselage tube used the quadratic as it have a simply geometry. On other hand, the fuselage used the tetrahedrons due the complex geometry.

[1] The numerical mesh is on Appendix A, Figure A.1.

3.5.2 Problem Setup

The problem setup follows the generation of the numerical mesh. This step is to define the boundary conditions and the forces applied on the structure.

The boundary conditions are defined according to the fuselage clamped at the wing connection. This boundary condition assumed that the wing is a rigid body. It can be a consequence of a higher stresses on the connection.

The problem setup studies three different analysis to confirm the preliminary sizing using the Static Structural model.

The first analysis was loading the fuselage with the inertia loads determined on Table 3.4. This forces were applied on the frames using the follow equation, Eq.(3.44), where F is the force and the F_i is the force on frame$i$[1].

$$F_i = \frac{F * (d_{i+1} - d_{F)}}{d_{i+1} - d_i} \; and \; F_{i+1} = \frac{F * (d_F - d_i)}{d_{i+1} - d_i} \tag{3.44}$$

The results of this transformation is shown on the, Table 3.12, which indicates, for each frame, the value of the frame force. The weight from the empennage support as well the horizontal tail and vertical tail were applied on the tube which are associate a moment, Table 3.13. The moment was determined using the distance between the CG and the tube.

Table 3.12 - Force in each frame of the fuselage.

	Force $[N]$
1 frame	8.72
2 frame	26.14
3 frame	1.40
4 frame	69.30
5 frame	1.33

Table 3.13 – Forces on tube.

	Units	**Moment** $[N.m]$
Weights force	$[N]$	5.63
Bending moment due the weights	$[N.m]$	0.38

The two other analysis it was used the maximum and minimum loads, Table 3.14, from both horizontal and vertical tail, determined previous.

[1] For a better understand use the Figure A.1.

Table 3.14 - Loads applied on the tail tube

	Loads	Force $[N]$	Moment $[N.m]$
1 – Maximum Loads	Horizontal tail	-6.76	0.396
	Vertical tail	14.57	2.045
2 – Minimum Loads	Horizontal tail	-34.60	2.025
	Vertical tail	-4.48	-0.629

3.5.3 Results

These results had the objective to see the maximum deformation, the maximum shear stress and the maximum normal stress to each loads applied on the structure.

Figure 3.11 shows the total structure deformation of all analyses. It is possible to see an increase deformation from the connection to the tail tube. The deformation for the inertia load is $1.19\ cm$ (Figure 3.11-a), for the minimum loads $3.35\ cm$ (Figure 3.11-b) and has predict the deformation is higher for the maximum loads $7.53\ cm$ (Figure 3.11-c). This is explained because it has the maximum lift force from both tails.

In Figure 3.12 shows the total shear stress of the structure. Regarding the inertia loads, Figure 3.12-a, it's possible to see that all fuselage have average shear stress of $4.21 \times 10^6\ Pa$ as it was determined on the preliminary sizing. It's also possible that the higher shear stress is located on the connection to the tail tube with a value of $1.56 \times 10^7\ Pa$. This two values are both below the admissible strength.

Regarding the shear stress to the maximum and minimum loads, Figure 3.12-b and Figure 3.12-c, it's possible to see that the connection has also the maximum shear stress. This is explained due the length between the boundary conditions and the tail tube. The maximum shear stress to the maximum and minimum loads is $3.03 \times 10^7\ Pa$ and $6.92 \times 10^7\ Pa$, respectively and both are below to the admissible strength.

The normal stress is represented on Figure 3.13 and it is possible to conclude that the connection has the higher stress. Regarding the inertia loads, Figure 3.13-a the maximum normal stress is $3.10 \times 10^7\ Pa$, for the minimum loads 5.84×10^7 and for the maximum loads $1.33 \times 10^8\ Pa$.

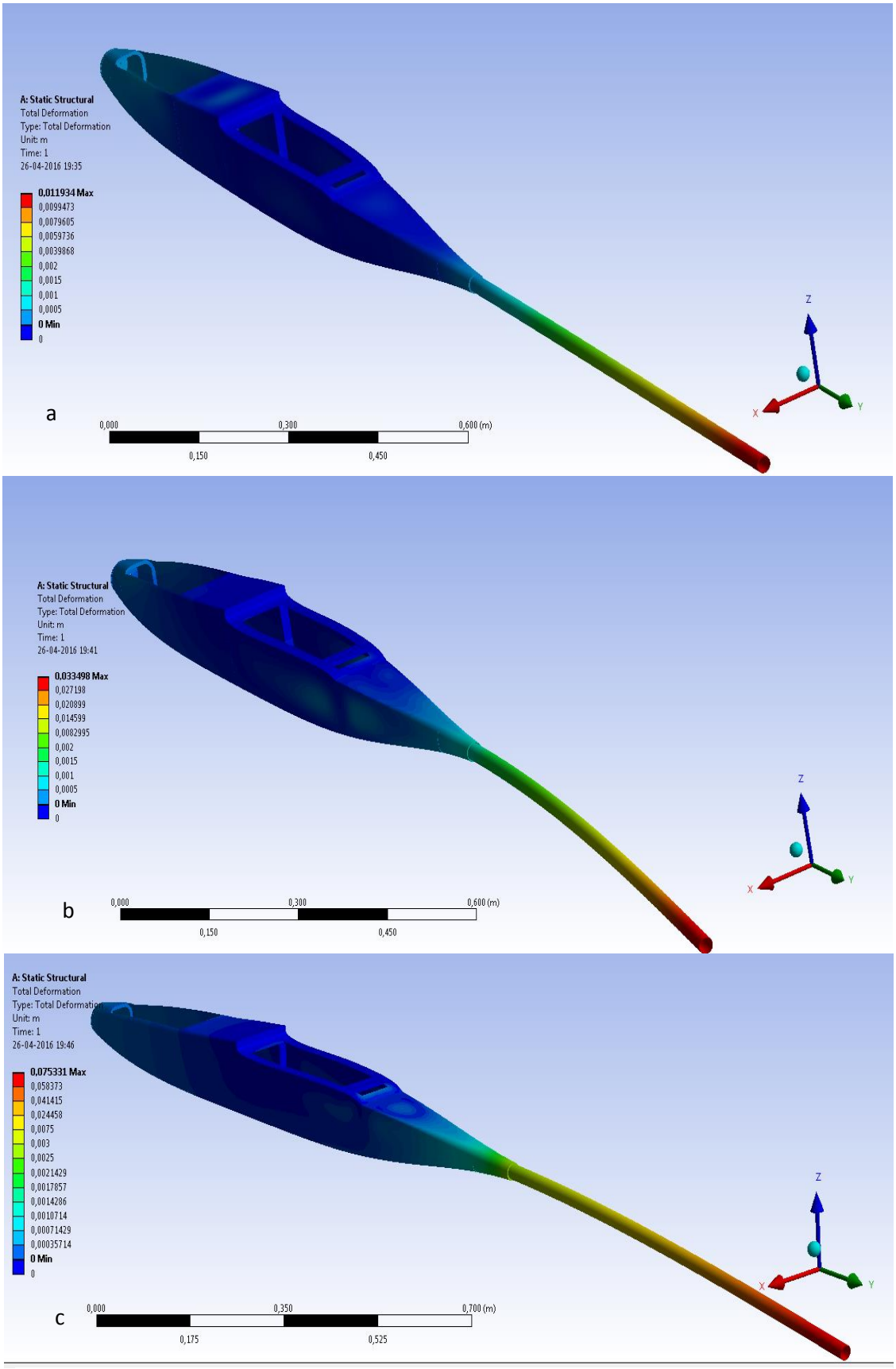

Figure 3.11 – Deformation: a) Inertia Loads, b) Minimum Loads, c) Maximum loads.

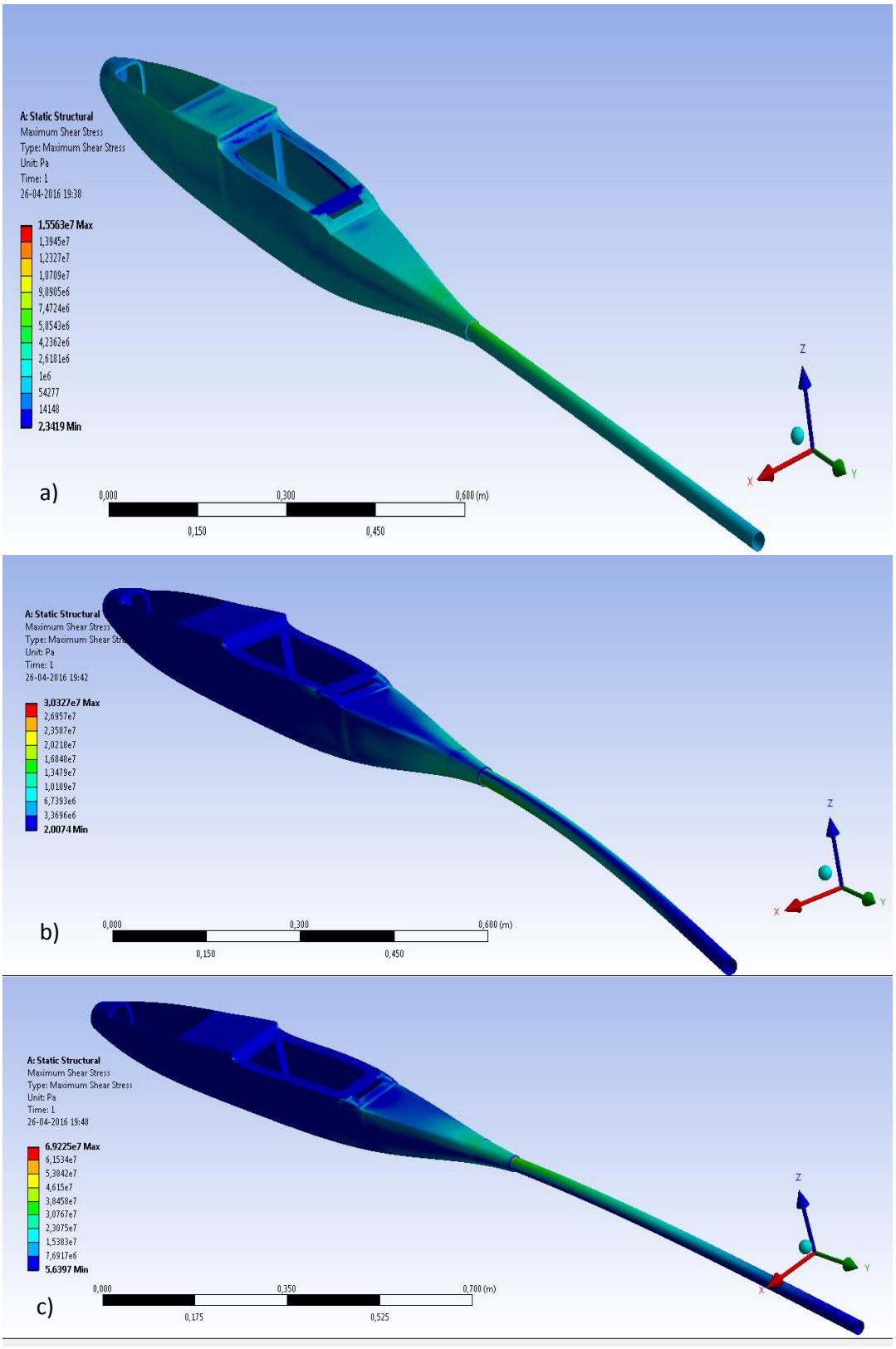

Figure 3.12 – Shear stress: a) Inertia Loads, b) Minimum Loads, c) Maximum loads.

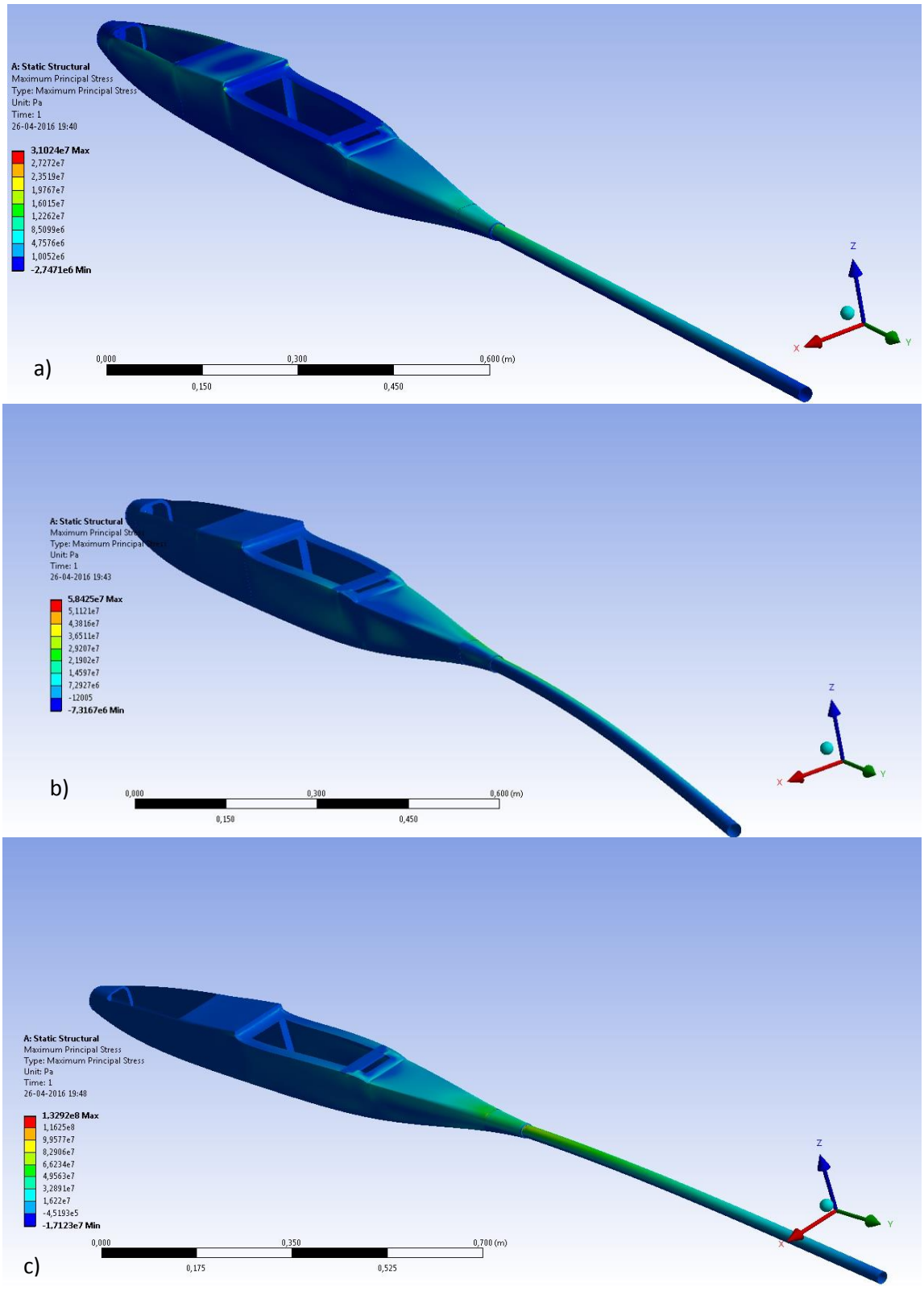

Figure 3.13 – Normal stress: a) Inertia Loads, b) Minimum Loads, c) Maximum loads.

Chapter 4: Manufacturing the LEEUAV

4.1 Manufacturing Method Selected

4.1.1 CNC milling machine

The CNC or Computer Numerical Control is a controlled machine by a prepared program containing coded alphanumeric data. The program controls both function and motions like the workpiece tool, the depth cut, speed and among others.

The CNC application include both machine tool and non-machine toll area[20]. The machine tool, the CNC is widely used for lathe, drill press, milling machine, laser, etc. The non-machine tool include the welding machines, coordinate measuring machine, etc.

The most popular milling CNC machines have a three degrees of freedom: X, Y and Z axis translation but in recent days a more sophisticated CNC milling machine was produce with five degrees of freedom where the cutting tool is manipulated not only translation but also in angular direction.

This project used a G-WEIKE WK1313[21] CNC milling machine that have a three degrees of freedom.

4.1.1.1 CNC milling Process

The CNC milling process is combining by using both CAD and CAM programs. In general terms, the CAD program draw the piece to milling and the CAM program built the process to the machine read and milling.

The numerical control is produce exporting the mould file in .STL with the following steps:

1. Input the raw material stock size and set the virtual part's coordinate origin.
2. Set which part feature it's needed, roughing, finishing or contour;
3. For each part feature select the appropriate tool from the library, and set the parameters necessary for machining that feature; typical parameters include spindle speed, depth of cut, federate, distance between toolpath, tool path pattern, etc;
4. Verify the programmed tool path(s) by running the CAM software's virtual machining;
5. Export the tool path(s) into an .NC program;
6. Set the origin using the features of the CNC milling machine
7. Start milling.

The cutting tool choice will determine the characteristics of the tooling marks on the mould as well the mould finishing. The most common tools are the end mill or ball nose end mill. This two are applied in different features due their geometry. The end mill has a flat geometry and it are often used for roughing and 2D cutting. On other hand, the ball nose end mill has a semi sphere at tool end and it are often used for finishing operations with complex surfaces like the moulds.

4.1.1.2 CNC milling Limitations

Before start milling with the CNC, two aspect must be under consideration: the maximum XYZ travel lengths and the design limitations. The table size can be a limitation to some jobs where the block to milling has bigger dimensions and it's impossible to do it in only one piece. The machine used have the follow cutting dimensions: $1.01m\ x\ 1.02m\ 0.5m$.

The design can be problem using the three degrees CNC, where some profiles can't be milling. An example in the Figure 4.1, where the B and C are the only design that can be milling. The other can only be milling if the machine has a five degree freedom.

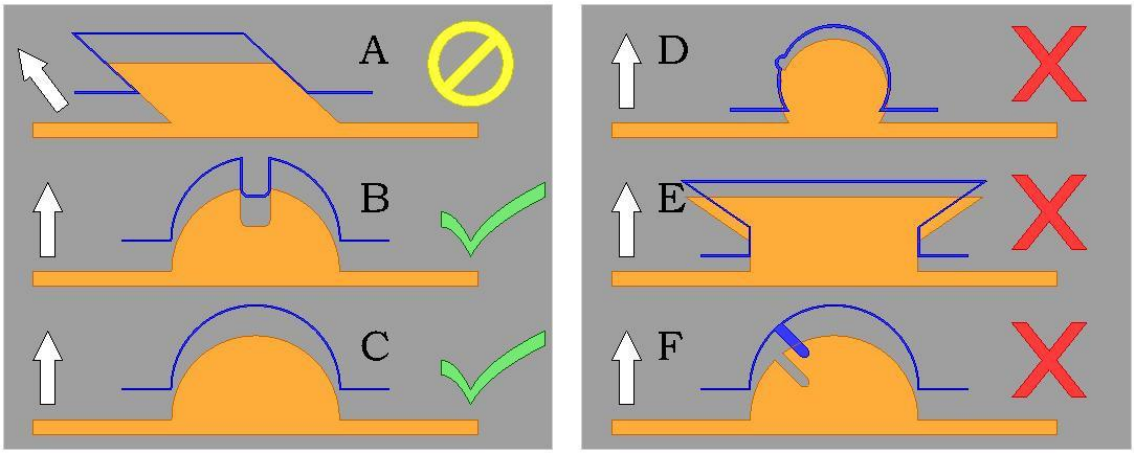

Figure 4.1 - Design limitations[32].

4.1.2 Laser Cutting Machine

The laser cutting machine[22] is a technology that uses a high-powered beam to cut the material based on computer-controlled parameters. As the laser starts cutting the material, everything on the direction is vaporized, burned or melted.

This technology has become an important part of manufacturing process due to some benefits. It has a high quality finishing, doesn't require too much time to cut, has a low waste of material and can be used to cut various types of materials like ceramic, wood, rubber, plastic and certain metals. One of the disadvantage of this technology is the fumes that can be released during the process that can be toxic and may be fatal. This machine must to be installed in a well-ventilated room to secure the environment to humans.

This technology have two formats: a gantry and a galvanometer system. The gantry system position the laser perpendicular to the material and the machine physically directs the beam

over its surface. In contrast, the galvanometer system use mirrored angles to reposition the laser beam and can cut as fast as $0.50\ m/s$.

This project used a G-WEIKE LG900[23], with a galvanometer system. The system has a refrigeration to cool the gas and it uses the air compressor to cool the laser and the material.

4.1.2.1 Process

The first step is to export the 2D files to the CAM program using a CAD program and then export to a .DXF file. The CAM program read the .DXF file and then we can start cutting. The program used is the Laser Cut and the process is explained as follow:

1. Reorganize, if it was export more than one draw;
2. Unit lines, this have to be made because when exporting to a .DXF file the draw is a group of line segments;
3. An offset with the dimensions of the laser width;
4. Put on program the values of cutting, Table 4.1, which depends on the material;
5. Before start cutting, the operator has to be in attention if the laser refrigeration is on and if the air compressor is pressurise;
6. Download the file to the machine;
7. Verify the dimensions and start cutting.

Table 4.1 - Reference values, to each material, for the laser cut

Material / thickness	**Speed** $[\boldsymbol{mm/s}]$	**Power** [%]	**Power Corner** [%]
Balsa – 1.6 mm	45	20	10
Balsa – 6 mm	30	70	35
Plywood – 2 mm	15	55	25
Plywood – 4 mm	20	75	30
Plywood – 6 mm	10	90	45

4.1.2.2 Limitations

Like the CNC, the laser has some limitations where is the table size and the material. The table size of the machine used is $0.90\ m\ x\ 0.60\ m$. As the laser cut use a high powered beam, some materials can't be cut because it can emit some toxic gas or damage the laser. The Table 4.2 refers some materials that can't be cut as well as the effects to the machine.

Table 4.2 - Materials that can't be cut on Laser

Material	Effects	Cause/Consequence
PVC(Poly Vinyl Chloride)	Emits pure chorine gas when cut.	This ruin the optics, cause the metal of the machine to corrode and ruin the motion control system
Polycarbonate (t≥1mm)	Cut very poorly, catch fire.	The frequency of the laser cut is infrared and the polycarbonate absorbs infrared radiation so the laser will be ineffective at cutting.
ABS	Emits cyanide gas and tends to melt.	This material tend to melt rather than vaporize, and has a higher change of catching fire and leaving behind melted gooey deposits on the vector cutting grid.
PolyStyrene Foam	Catches fire	It melts, it catches fire.
PolyPropylene Foam	Catches fire	Like the PolyStyrene, it melts and catches fire.
Fiberglass	Emit fumes	The laser can't cut the glass and the resin emit fumes.
Carbon fiber	Emit fumes	It emits noxious fumes and the laser can't cut.

4.1.3 Vacuum Bagging Method

The fabrication process is the most important step in the application of composites materials, it because any failure on the manufacturing process affects the final properties of the composite structure.

There are several manufacturing techniques for the application of composite materials, has seen in Chapter 1 but for this project the method applied was the vacuum bagging method.

The vacuum bagging is a simple method which uses the atmospheric pressure to hold the laminate to a mould until the resin cures.

This method used a variety of material to complete the vacuum system and assist in laminating process. These materials are listed and described below.

- Release agent: is chemical product to prevent the epoxy to stick into the mould. The application is usually put in up to 10 layers with 15 minutes interval;
- Peel ply: is a finely woven polyester fabric. It is used to give the laminate a rough surface to be possible a connection to other structure;
- Release film: is a perforated plastic film and helps hold the resin into the laminate;
- Breather material: is a thick layer of cloth to collect the excess of resin;
- Vacuum bag: is a tiny plastic which involves the mould to provide the necessary vacuum environment;
- Sea tape: is a mastic, to stick the vacuum bag, to provide a continuous air sealant between the bag and the mould.

The Figure 4.2 shows a schematic process of the vacuum bagging.

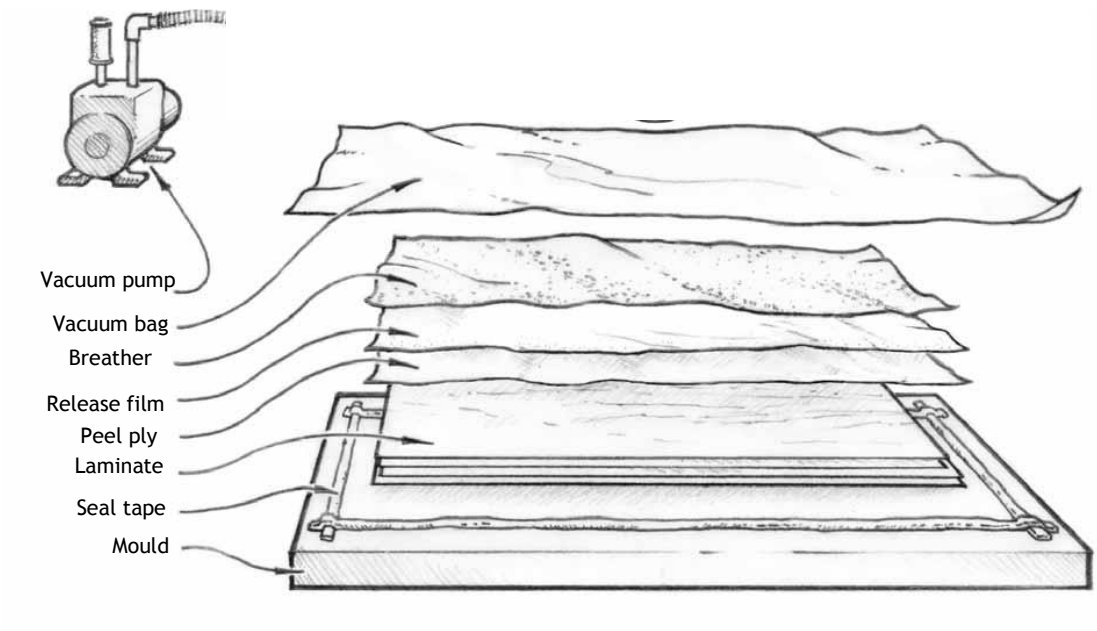

Figure 4.2 - Typical components of a vacuum bagging system[33].

4.1.4 Materials and Tools

The materials used during the manufacture are listed on Table 4.3.

Table 4.3 - Material used during the manufacturing

Materials	Description
Biresin®CR 122/CH 122	Lay-up Resin/Hardener
Biresin®Kleber brown	Adhesive for SikaBlock®.
Biresin®Spachtel braun	Putty for SikaBlock®.
Carbon Fibre	A 90 g/cm^2 and 190 g/cm^2 carbon fibre.
Carbon fibre tape	Carbon fibre tape with xxx width.
Cyanoacrylate adhesive	Super glue.
Epoxy Glue	A 10 minutes and 30 minutes work time using two components.
Fibre Glass	A 60 g/cm^2 fibre glass.
General material	Latex gloves, mixing cups, tape, eye protection, masks, etc.
Polystyrene foam	Extruded polystyrene.
SikaBlock® M700	70% density polyurethane modelling board.
Wet/Dry Sandpaper	Different grids.
Wood	Plywood and balsa with different dimensions.

For the UAV fabrication, the glue is the principal adhesive. For this project two glues were used in different locations, the two components epoxy and the cyanoacrylate.

The two components epoxy work in any place, because it has good properties when present to shear or normal strength[24]. On other hand, the cyanoacrylate glue works better in tensile applications.

Several tools were necessary during the manufacturing and are listed on Table 4.4.

Table 4.4 - Tools used during the manufacturing

Tools	Description
Cutting instruments	Sharp bladed (X-Acto) and shears tools.
General tools	Clamp tool, Dremel,
Measuring equipment	Measuring tape, ruler, and callipers.
Sanding blocks	Support for sanding papers.
Vacuum components	Seal tape, breather, peel ply, release film, vacuum bag, release agent.
Vacuum pump	Vacuum pump with all the utilities.

These materials and tools were repeatedly used in the various phases of construction as it will be explained in further chapters.

4.2 Fuselage and Tail Support

This chapter explains the different stages to manufacturing the fuselage and the tail support.

4.2.1 Mould Creation

The mould creation process is one of the most important phases of the fabrication because this will define how the structure will be. The material chosen is the SikaBlock® M700[25] with nominal dimensions $1500\,x\,500\,x\,50\,mm$. This is a low density polyurethane with a high capability of machining.

The fuselage mould was divided in two symmetric moulds to can be milled using the 3 axis CNC milling machine. These moulds were modified in some aspects to help the later fabrication. It was extend both access hatches to be able the access to the interior, it was drew a groove with the same diameter as the tail tube with $40\,cm$ length to help position the fuselage tube and it was draw four holes with $8\,mm$ of diameter, on each edge, to help placed the two symmetric moulds.

These modifications increase the length of the fuselage mould up to $1.50\,m$ which pass the cutting limits of the CNC milling machine. So it was needed to divided the mould into two different parts, one with $1.0\,m$ and other with $0.50\,m$.

After defining the two moulds, the numerical control using the CAM program can be started. It was used two features, the roughing and the finishing[1] with a $10\ mm$ end mill and a $6\ mm$ ball nose respectively, Figure 4.3.

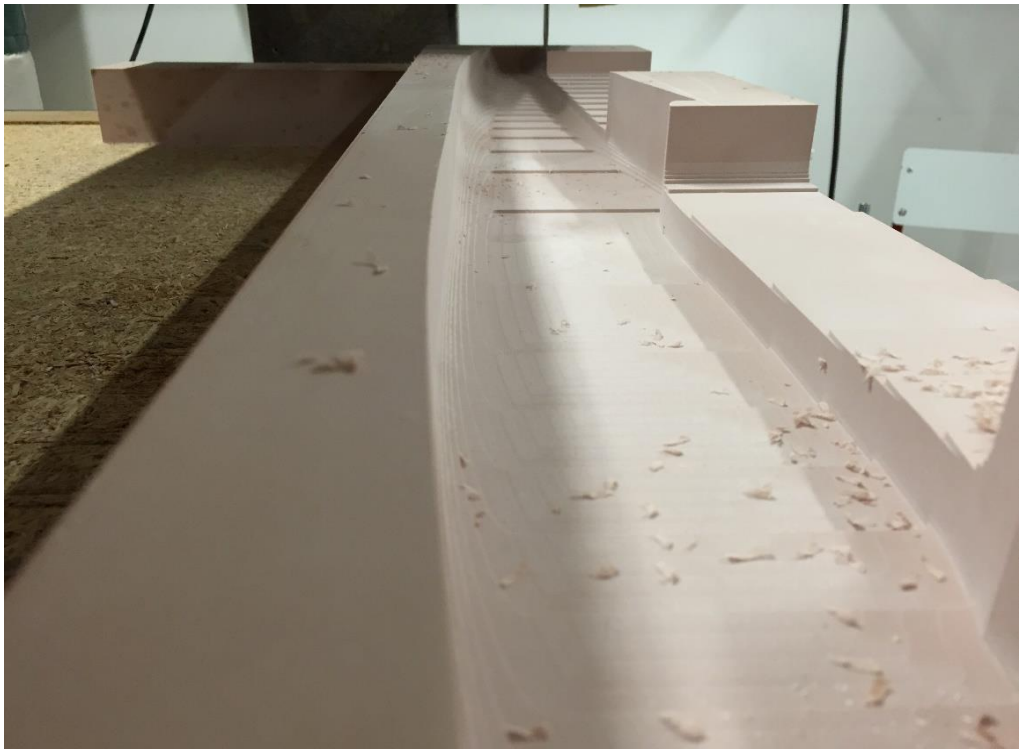

Figure 4.3 - Roughing finished on the right-fuselage mould.

Once the two parts of the fuselage moulds have been milled the Biresin Kleber was used to join, Figure 4.4. This adhesive is recommended by the producer to join SikaBlock® products.

The moulds of the empennage support as well the fuselage access hatch had the same procedure and have the configuration show on the Figure 4.5.The CNC milling machine don't give a perfect finishing so it was used different grids of wet sandpapers until it had a smooth and cleaning surface. After this, the release agent was applied 10 times in a 15 minutes interval[2].

[1] The parameters for machining using this material is on Appendix B., Table B.0.6.
[2] The number of layers were defineddefine by the producer.

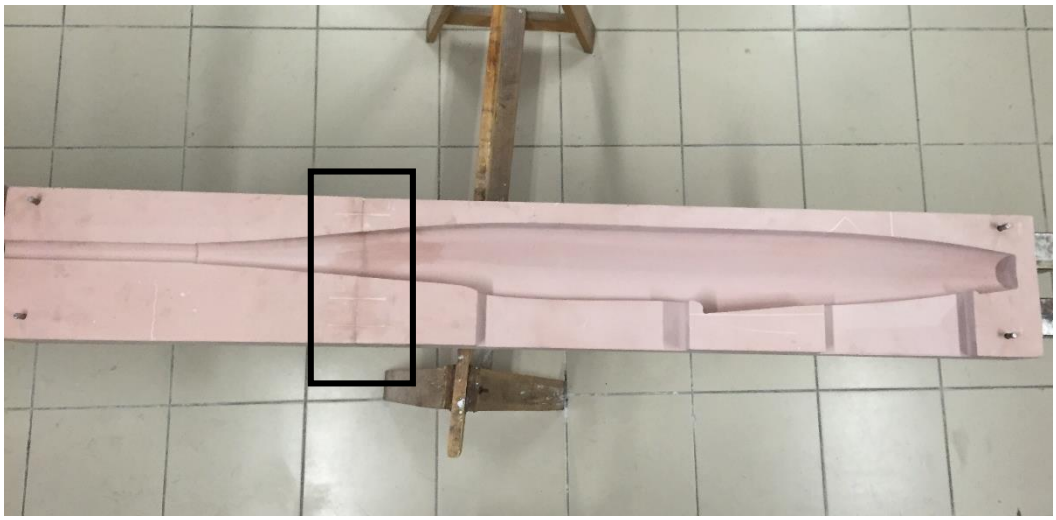

Figure 4.5 – The right-fuselage mould after be adhesive.

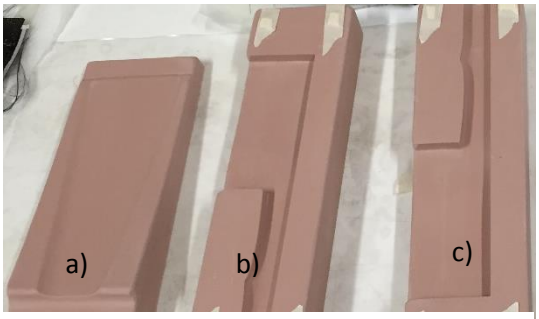

Figure 4.4 – Fuselage access hatch (a) and empennage support [b) and c)] moulds finished.

4.2.2 Resin Lay-up

The Lay-up process was a coordinated group work requiring three a four individuals. Although it was possible more pairs of hands but the management of too many people it's impossible as the room became crowed. This process also requires some knowledge about the lay-up process so a resume and a preparation was made.

This process consists placing the layers of carbon fibre and fibre glass with the indications of the structure analysis. The fuselage uses one layer of fibre glass, two layers of carbon fibre (one of 90 g/cm^2 and other 190 g/cm^2) and three layers of carbon fibre on the last 10 cm of the fuselage. The empennage support as well the access hatch use two layers of carbon fibre (both with 90 g/cm^2).

The epoxy needed for the process is equal to the weight of carbon fibre plus fibre glass needed which have a 70% to 30% ratio of the weight for the epoxy plus hardener, respectively. The epoxy used was the Biresin®CR 122, it can be used with some hardeners referenced by the producer. In this case the hardener use was the Biresin®CH 122 and have a work time about 45 minutes. The producer also says that this is adequate to standard lay-up so it suits perfectly to the work desired.

Before initiating the lay-up process some important steps have to be done. Firstly, and more important, is to organize the necessary materials and tools on the work area. Secondary, is to cut all the carbon fibers and fibre glass needed as well the peel ply, the release film, the breather and the vacuum bag. And finally is to place the double-sided vacuum seal tape along the outside edges of the mould on a clean glass table.

During the lay-up process the layers were placed as follow: fibre glass, 90 g/cm^2 carbon fibre and 190 g/cm^2 carbon fibre. While placing the layers of carbon fibre, a precaution on the sharp edges have to be made requiring some relief cuts so it could conform the curvature, Figure 4.6.

Figure 4.6 – Left-fuselage lay-up resin.

The empennage support and the access hatch have an identical process as explained previous.

4.2.3 Vacuum Bagging Process

The vacuum sealed bag as well the peel ply, the release film and the breather were placed Figure 4.7 -a. As, on the application of the carbon fibre, these materials have to suffer some relief cuts on the sharp edges of the fuselage. In some edges that are too sharp the material can't cover and small strips of the material have to be added. This was made especially for peel ply which didn't have too much elasticity as the other materials and to the breather to be impossible the direct contact of the resin with the vacuum bag. Not be forgotten while placing the vacuum bag on the seal tape, to put the valve into the mould with some small pieces of breather to protect the vacuum bomb. The vacuum was applied, Figure 4.7- b, until the bag as almost nothing air to help position the vacuum bag inside the mould without rough and to check if the laminate is all compress to the mould to prevent the bridging[1].

The pressure on the vacuum pump was around 8 bars. This pressure was maintained during the cure process, which lasted 24 hours.

[1] The bridging is a natural consequence using the lay-up and the vacuum system. It occurs when the mould have complex curvatures where the laminate does not fully compress to the mould, and in the gaps the resin will fill and gives to the laminate a visible resin-rich pockets on the surface. This adds to the part an unnecessary weight and also it are subject to crack especially if it is subject to stress.

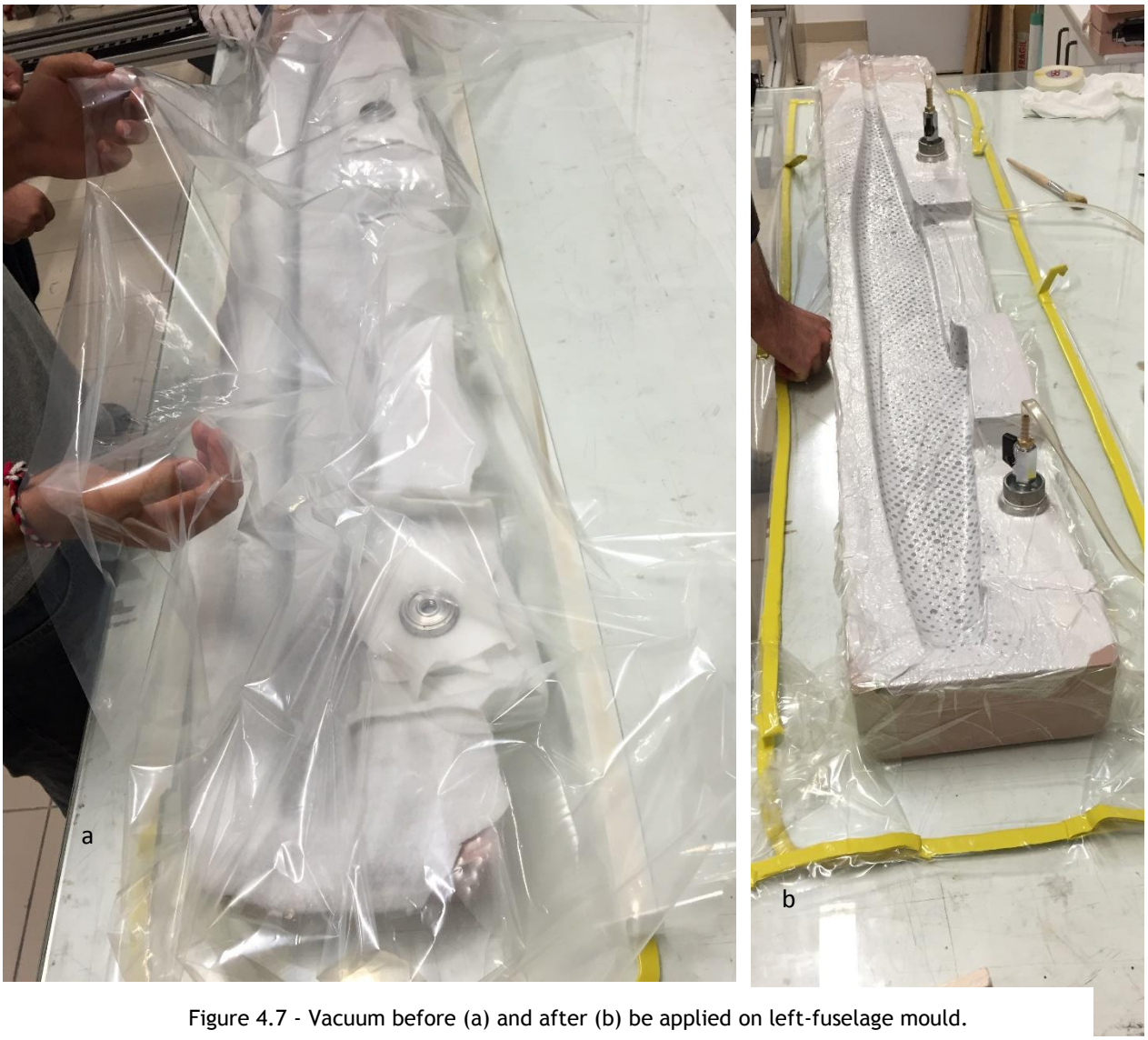

Figure 4.7 - Vacuum before (a) and after (b) be applied on left-fuselage mould.

4.2.3.2 De-mold

The primary tool used to release the part from the mould was compressed air. But after using the compressed air the breather, the peel ply and the release film have to be removed. The compressed air was injected evenly around the flange causing the laminate to “pop” of the mould (Figure 4.8). The empennage and the access hatch mould was de-molded in a similar way.

Figure 4.8 – Left-Fuselage de-moulded.

4.2.4 Fuselage

The two laminate parts of the fuselage have some over edges and to can be joined it had to be removed by using an X-Acto. Afterwards, the parts were placed into the mould, and using a sanding block, the edges were smooth until it had an identical profile to the mould.

Before joining the two half's, the fuselage tube needs to be placed, due to the small space on the fuselage. Initial the fuselage tube was attached to the frame tube using the 10minutes epoxy glue. Then, using the same epoxy glue, the fuselage tube was attached to the fuselage with the support of the tail tube and the groove, made on the mould, to help positioning the fuselage tube, Figure 4.9. It was added some lead weight to have some pressure while it was drying.

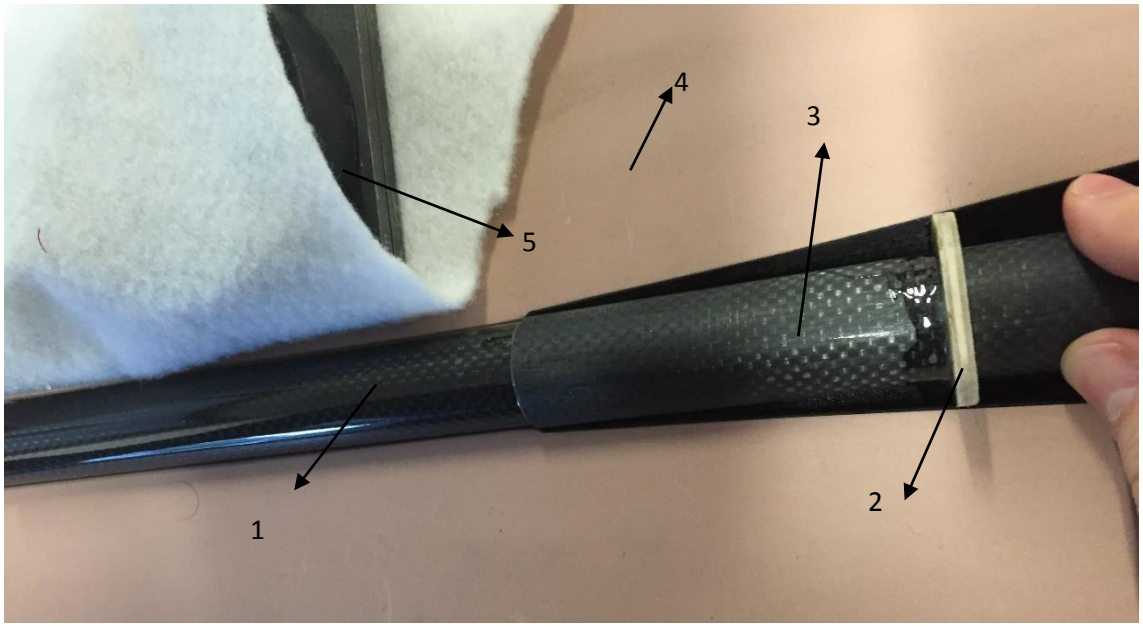

Figure 4.9 - Fuselage tube in position (1-Tail tube; 2-Tube frame; 3-Fuselage tube; 4-Fuselage mould; 5-Lead weight).

The fuselage was joined using a carbon fibre tape with $4\ cm$ width. This process use the four holes with four bars to secure the right position of the two moulds. The carbon fibre tape is impregnated, on a clean table, and placed between the union of the two half's. Due to the short space inside the fuselage, the carbon tape was first placed on one fuselage mould, Figure 4.10-a, and using the four bars as reference, the other half mould was placed. It was used some lead weight, to make pressure, and a strip, with the same width of the tape, of polystyrene foam, to spread the force and to avoid the weights to be in direct contact to the impregnated carbon fibre tape. The joined fuselage is on Figure 4.10-b.

The portion between the tube frame and the rear of the fuselage hasn't be joined due to the location of the fuselage tube. So it was added small strips of carbon fibre using a chamfer with$10\ cm$, Figure 4.11.

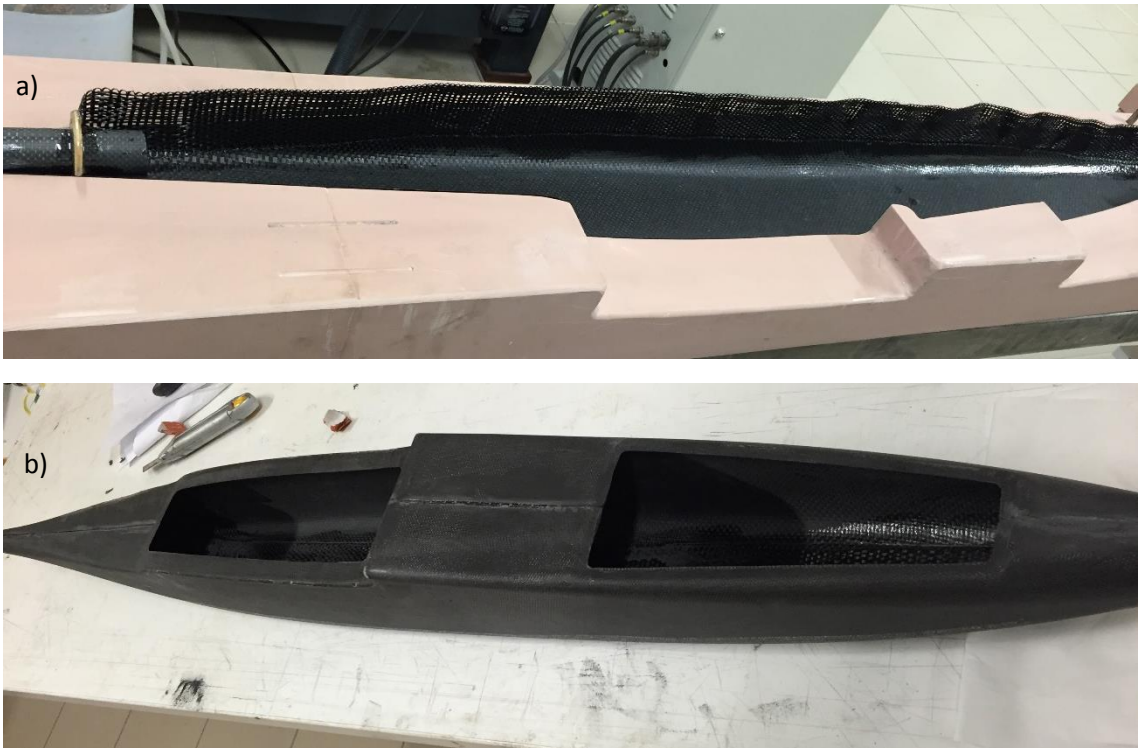

Figure 4.10 – Fuselage before (a) and after (b) be joined.

Figure 4.11 - Chamfer on the fuselage top.

The internal structure of the fuselage, frames and longerons, were created using the laser cut machine. They were placed on the fuselage with the 30 minutes epoxy glue.

4.2.5 Tail Support

The tail support was joined similarly to the fuselage. The two half's were mated and joined together via the lay-up of a reinforcement carbon fibre strip with $1.5\ cm$ width.The empennage support after being joined, shows some imperfections which are caused by a small movement of the moulds during the cure time.

The frames were cut, using the laser cut machine and glued in the same locations as the CAD drawing. The Figure 4.12 shows the final configuration of the empennage support as well as a guide to the servo wires from the vertical tail.

Figure 4.12 - Empennage support complete.

4.3 Tail

4.3.1 Manufacturing method

The first process is to create a bed to help placing all the internal structure. The bed is the lower surface of the aerofoil and it was milled using a polystyrene foam with the CNC milling machine[1] Figure 4.13. The internal structure of both tails include the leading edge, the ribs, the main spar, and the trailing edge.

Figure 4.13 –Horizontal (a) and vertical (b) tail bed.

The leading edge of both tails, as well as, the elevator and the rudder had the same process. It was used a sheet of balsa with the same dimensions of the leading edge with a profile on each edge to secure the geometry. The major material was removed using a scalpel and a sandpaper to smooth the surface. The figure Figure 4.14 shows the finished leading edges.

The horizontal tail spar is composed by a sheet of plywood and balsa and two carbon fibre strip. The sheets of wood were cut using the laser cutting machine and glued using the 10 minutes epoxy. The carbon fibre strip was cut using a dremel and glued in each edge of the spar.

The vertical main spar were placed similarly to the horizontal tail spar. The balsa sheet and the carbon fibre strip were cut using the laser cut and the dremel, respectively. The two parts were joined using the 10 minutes epoxy glue.

The ribs and the trailing edge were manufacture using the laser cut machine with the 1.6 mm balsa wood.

[1] The parameters for machining using this material is on Appendix B., Table B.6.

Figure 4.14 - Horizontal and vertical tail leading edges.

The integration of this structures results in the horizontal and the vertical tail which are explained on the next subchapters.

4.3.2 Horizontal tail

The method to build the horizontal is like a “puzzle”. Using the CAD drawing as a reference, the internal structures were placed with the follow procedure:

The skin was firstly placed on the mould using various pins to secure the right position. Then using the cyanoacrylate glue the spar was placed on one edge of the skin.

The ribs, as well as, the servo structure were measured using the CAD drawing and marked in the skin. In each rib was used a small triangle to ensure that they were vertically to the mould, Figure 4.15 -a.

The two servo structures are composed by two ribs and two stringers. The ribs were already placed in position. For the stringers, first the servo was placed to ensure the dimensions and then it was glued into the skin and ribs, Figure 4.15 –b.

The connection structure is composed by the reinforcement on the main spar and the screw reinforcement near the leading edge. The reinforcement of the spar was already placed. Regarding the screw reinforcement it glued between the two ribs, Figure 4.15 –c.

The skin was glued on top of the ribs and the spar using the 10 minutes epoxy. The epoxy was used to ensure the right position of the skin. The epoxy is suggested to be used in these application due to its working time. Finished the fix structure, the leading edge was placed.

In the elevator the process was similar. First the leading edge was placed parallel to main spar. The ribs location were marked on the mould using the CAD drawing and it was glued to the leading edge using the cyanoacrylate, Figure 4.15-d.

The trailing edge is composed by two balsa sheets placed on the ribs slot. Firstly it was glued one balsa sheet on the bottom of the ribs, Figure 4.15- e. Secondly it was trimming this balsa

sheet until it is tangent to the ribs and finally the second balsa sheet was glued on the top the rib.

The Figure 4.15 –f and g shows the integration of the internal structures of both flexible and fix structure.

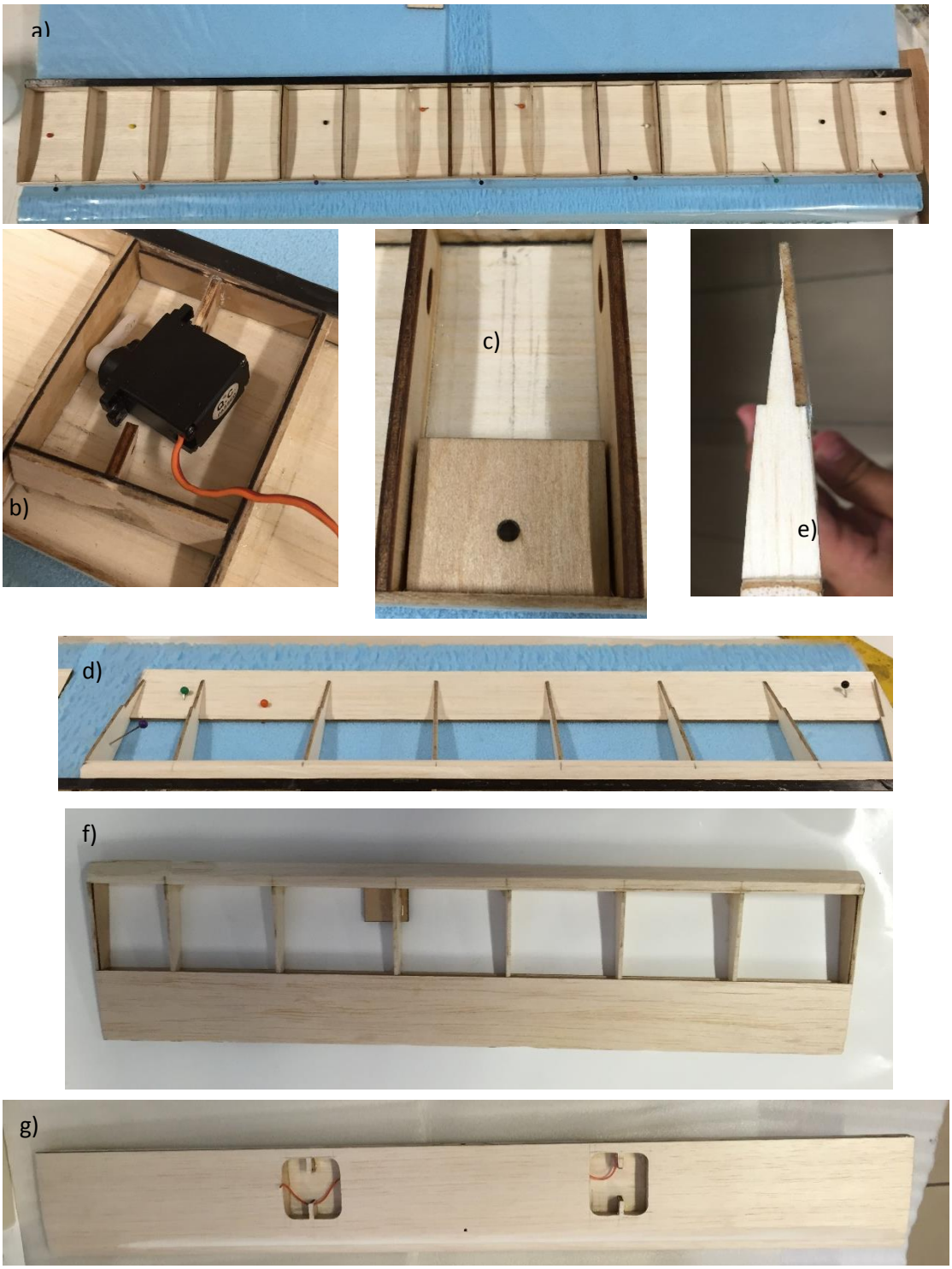

Figure 4.15 –Horizontal tail manufacturing steps.

4.3.3 Vertical tail

The vertical tail had the same method as the horizontal tail. Firstly the skin was placed on the bed using some pins to secure it into the mould. The spar was then glued using the cyanoacrylate on the skin extremity, Figure 4.16 -a.

The ribs locations were measured and marked using the reference and glued in the skin with a small triangle to ensure the verticality. The ribs of the serve structure were placed too.

The servo structure is composed by the two ribs and two the stringers. As the ribs were already placed, the stringers were glued using the servo with reference to ensure the right dimensions of the structure, Figure 4.16 -b.

After placing all the internal structure the top skin was glued using the epoxy glue and finally the leading edge was placed in position using the cyanoacrylate.

For the elevator, the ribs were market and glued into the leading edge, Figure 4.16 -c. Then using the two balsa sheets the trailing edge was trimming and glued, Figure 4.16 –d.

The Figure 4.0.16–e) and f) shows the integration of the internal structures of both flexible an fix structure.

Figure 4.16 – Vertical tail manufacturing steps.

Chapter 5: Assembly the LEEUAV

This chapter is the result of this thesis which is the conception of a Long Endurance Electric UAV structure. It explains the different connections between the Wing-Fuselage, Fuselage-Tail tube and the Tail support-Tail.

5.1 Assembly

5.1.1 Tail tube

The LEEUAV principal connection is between the tail tube and the fuselage because it is the link to both control surfaces.

This connection was made of two sheets of plywood, a cross, which will be connected to the fuselage tube and a screw on the datum of the fuselage. The cross, as explained previous, is composed by two sheets of plywood with $2\ mm$ thick, Figure 5.1 -a. It was glued on the fuselage tube with the 10 minutes epoxy glue, Figure 5.1 -b. But on the first attempt to connect the tail tube the cross unglued. This is explained due the small contact area between the cross and the fuselage tube.

The area of contact was increased using carbon fibre and a portion of the fuselage tube. The cross was insert inside the tube and some strips of impregnate carbon fibre were insert between the cross and the tube. This was made to the sides of the four connection points, Figure 5.1 -c. After position the layers of carbon fibre, a release agent had to be applied on the fuselage tube.

The other connecting point was the wood screw on the datum of the fuselage to prevent the tail tube to slice out. But to screw the screw a reinforcement of plywood was added on the tail tube with $4\ mm$ of depth.

5.1.2 Tail

The horizontal tail is connected to the empennage support using the two carbon fibre rod and a screw. Firstly was measure and market the location of the two holes of both carbon fibre rod in the empennage support. Using a dremel with a $2\ mm$ drill the two holes were made. In this step it was needed to ensure the full contact of the tail with the support. Before made the leading edge screw hole, it was used two triangles to ensure the perpendicular position to the lateral face of the empennage support.

The vertical tail as definition is always perpendicular to the horizontal tail. This was made fixing the vertical as well the horizontal tail with a tape on a table. Then it was measure the distance between both tails tip until it have the same distance, Figure 5.1 -d.

5.1.3 Empennage Support

The empennage support with both tails fixed was glued in the tube using 10 minutes epoxy glue. After can be glued, the wing was placed to ensure that the horizontal tail was parallel, Figure 5.1 -e.

5.1.5 Wing

The central-wing have two connections points with the fuselage, one is the two carbon fibre rod and other is the two screws. The holes to the carbon fibre rod were made previously made to can place correctly the empennage support.

The wing to be placed on the right position it needs to be parallel to the horizontal tail. This was made measuring the length between the CG of the horizontal tail and the CG of the central wing using a fish line. It was needed several attempts to guarantee the final position of the wing.

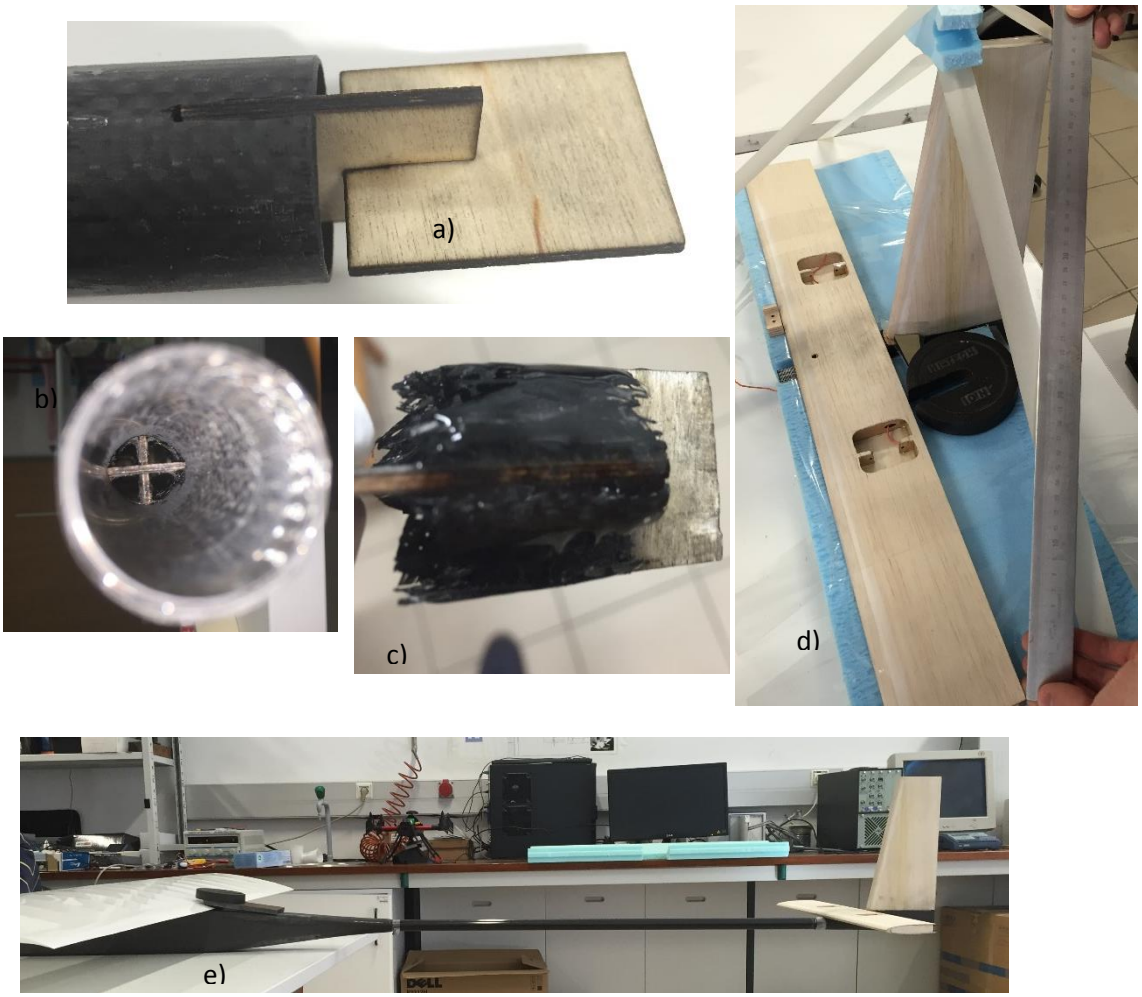

Figure 5.1 - LEEUAV assembly.

5.2 Structural Testing

The structural testing was perform with the objective to predict the maximum deformation of the fuselage and the empennage support and also to confirm the structural analysis. The test was performed fixing the fuselage and loading the empennage support.

The fuselage supports were positioned on the connections between the wing and the fuselage to simulate the deformation during the flight, Figure 5.2. The support have the same connection points as the wing which is two carbon fibre rods and two screws and it was fixed to a table using 4 clamps in each support.

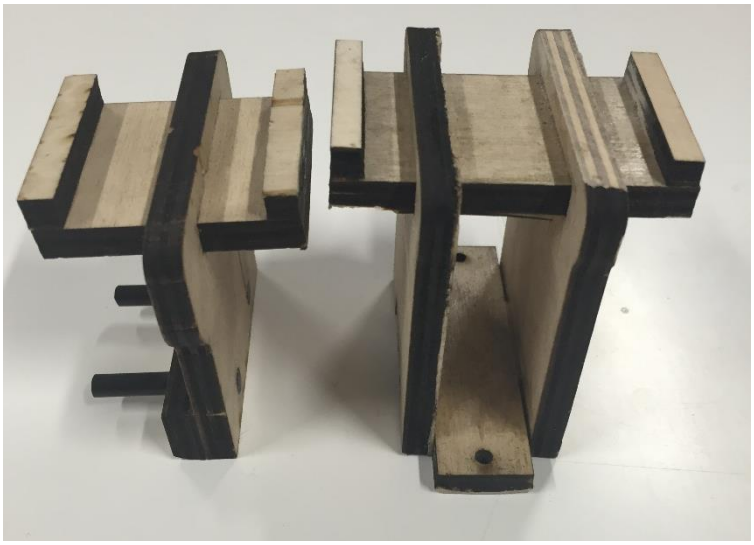

Figure 5.2 – Fuselage supports

The empennage support was loaded with the maximum and minimum loads from the horizontal tail. This loads were already determined in the 3.2 subchapter and it has the follow values: $L_H = -6.76\ N$ and $L_H = -34.60\ N$.

The test, Figure 5.3, was perform testing nine different weights (0 Kg, 0.5 Kg, 1.0 Kg, 1.5 Kg, 2.0 Kg, 2.5 Kg, 3.0 Kg, 3.5 Kg and 3.7 Kg) to both negative and positive lift force with the objective of predict the deformation on the different flight stages. The deformation was measure using a scale and a camera.

The Table 5.1 shows the deformation of the fuselage and the empennage support

Table 5.1 – Structural test results

Weight $[Kg]$	Support $[cm]$
0.0	0.00
0.5	0.9
1.0	1.5
1.5	2.3
2.0	3.3
2.5	4.1
3.0	5.0
3.5	5.8
3.7	6.2

The results of this test shows that to the maximum negative force the maximum deformation is $6.2\ cm$. This value represents a $2.98°$ deflection. Comparing this values with the obtained by the FEM method, $7.52\ cm$, it's possible to conclude that the structure manufacture is more rigid than the used in the method. This is explained for two reasons: one is that the addition of the three layers of carbon fibre on the chamfer could increases the stiffness on the connection; other is that the two fuselage supports could move when adding the weights on the empennage support, which may cause a bad measure reading of the deformation.

This deflection can be prejudicial to the control of the UAV. It can induce a higher angle of attack on the tail producing a higher lift which cause a nose pitch up. It can also affect the trimming of the UAV by changing the deflection of the elevator.

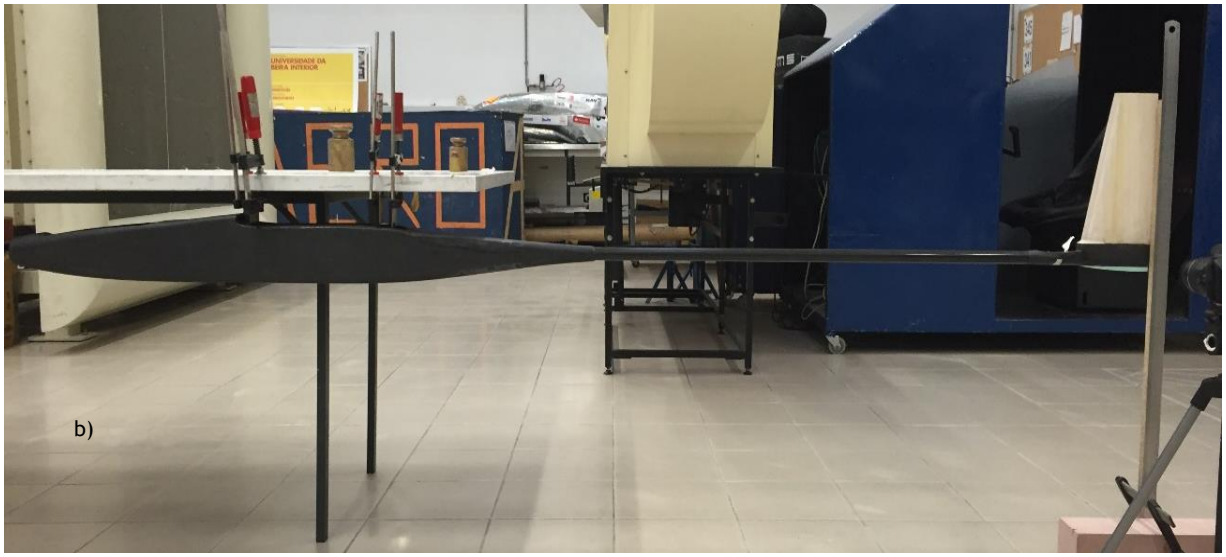

Figure 5.3 - Fuselage ready to test the positive lift force.

5.3 LEEUAV

After joining all the structures an aerodynamic surface was given using the solar film. Then the servos and the respectively wires were positioned. The final LEEUAV have the final configuration shown in Figure 5.4, Figure 5.5 and Figure 5.6.

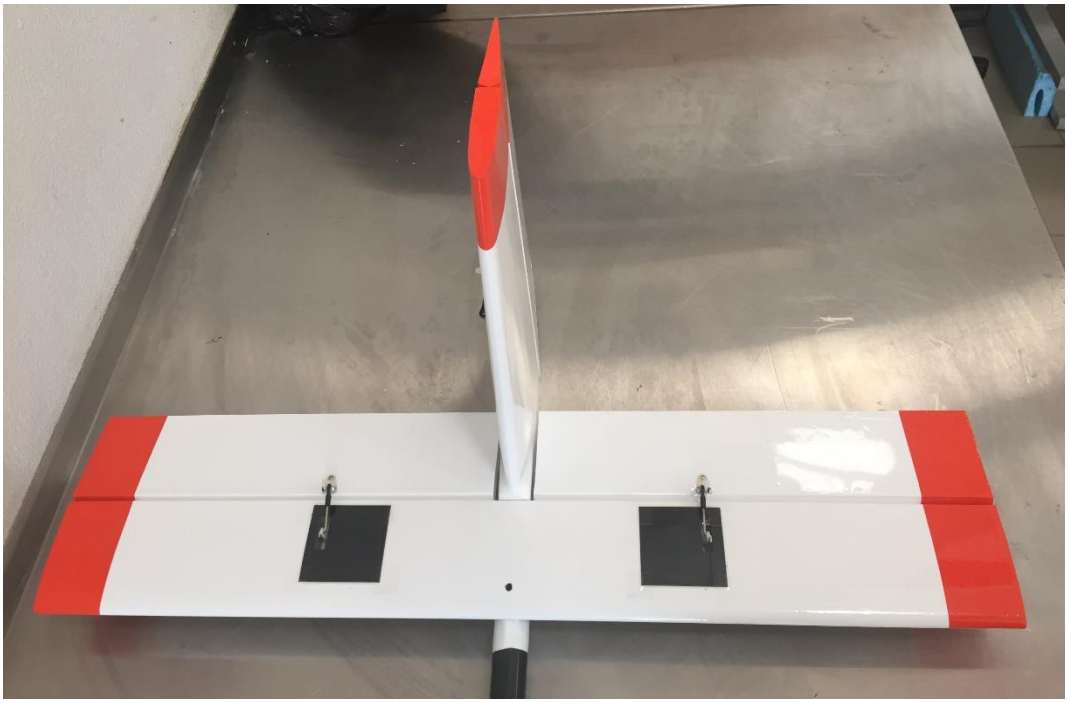

Figure 5.4 – LEEUAV tail.

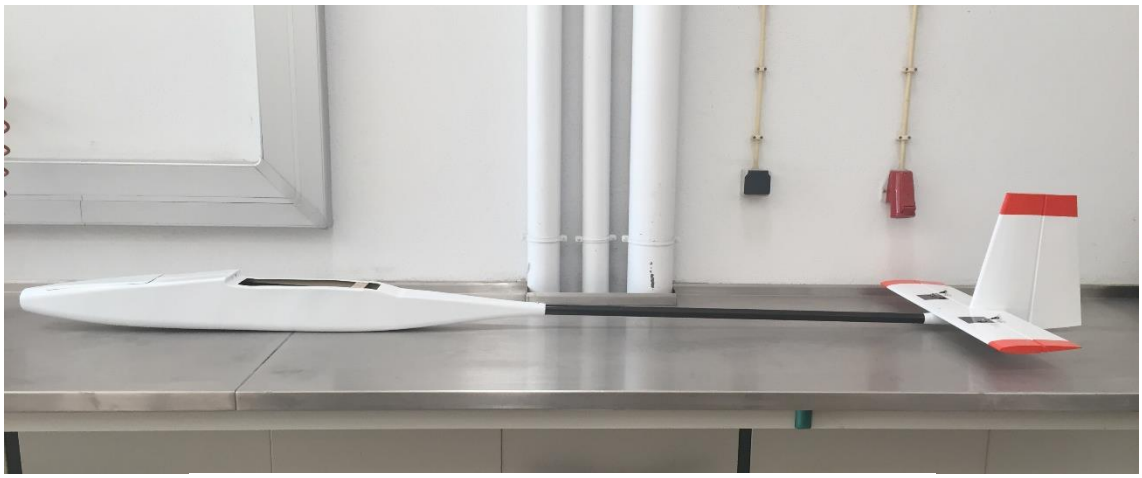

Figure 5.5 – LEEUAV frame.

Figure 5.6 – Completed LEEUAV.

The Table 5.2 shows the final mass of all structures comparing with the parametric study[9]. By comparing the two mass, it can conclude that the expect mass, from the parametric study was not the reals. It is explained by the reinforcements added during the manufacturing. Regarding the final mass of the LEEUAV, the values are a bit different which is explained due the final mass has all the components like servos, wires, solar film.

Table 5.2 – Final mass for each structure

Structure	Parametric study mass $[Kg]$	Final mass $[Kg]$
Horizontal tail	0.0857	0.1068
Vertical tail	0.0663	0.0607
Tail support	[–]	0.0338
Fuselage	0.531	0.434
LEEUAV	0.604	1.068

Chapter 6: Conclusion

6.1 Achievements

This project includes two different works. The first was the design of a lightweight structure for a long endurance electric UAV and the second its manufacturing.

The design includes the configuration and analysis of the structure. The configuration of the UAV includes two structures using carbon fibre, the fuselage and the empennage support and two other using wood, horizontal and vertical tail. Because the UAV needs to fit on a regular car trunk, the tail tube had to be detachable from the fuselage. The best solution for this connection was to use a cross.

The structure analysis was performed for both composite structures. From the preliminary analysis resulted a 0.4 mm thickness of the fuselage and a 0.94 mm thickness of the connection to the tail tube. On the other hand, the empennage support only needs 0.26 mm thickness of carbon fibre. The FEM analysis, using the software ANSYS®, confirms the results of the preliminary analysis and also confirms the dimensions used on the internal structure and the connection solution as well.

The manufacturing used two different methods. For the composite structures the lay-up and vacuum bagging method with a mould was used and for the empennages the balsa wood construction.

The structural testing was performed to test and confirm the results of the application of both the analysis and the manufacturing method on this project. The result for this test shows that, for the maximum horizontal load, the empennage support has a deflection of $6.02\ cm$.

Finally, it can be concluded that the objective of this work was reached with the development and construction of a lightweight LEEUAV with $1.068\ Kg$.

This project gave to the developer important practical experience in composite manufacturing, in the manufacturing of a light weight UAV and on the control of CNC milling machine.

6.2 Future Work

This project can be extended with the following items:

1. The flight test needs to be performed to confirm both structure analysis and manufacturing methods;
2. Perform a flight test using the solar panels to confirm the versatility of this project.

Bibliography

[1] "Greenhouse gas emission statistics - Statistics Explained." [Online]. Available: http://ec.europa.eu/eurostat/statistics-explained/index.php/Greenhouse_gas_emission_statistics. [Accessed: 15-Apr-2016].

[2] C. European, "Climate change : Commission proposes bringing air transport into EU Emissions Trading Scheme," *Press Release IP/06/1862*, no. December 2006, p. 2, 2006.

[3] R. J. Boucher and A. F. Inc., "History of Solar Flight," *AIAA/SAE/ASME 20th Jt. Propuls. Conf.*, vol. c, no. July, pp. 1–22, 1984.

[4] V. K. Vashishtha, A. Kumar, R. Makade, and S. Lata, "Solar Power the Future of Aviation Industry," *Int. J. Eng. Sci. Technol.*, vol. 3, no. 3, pp. 2051–2058, 2011.

[5] A. A. Baker, S. Dutton, and D. Kelly, *Composite materials for aircraft structures*. 2004.

[6] C. Materials, R. Aerospace, and W. Creation, "Wealth Creation Composite Materials Revolutionise," *Manual*, no. 36, pp. 25–27, 2008.

[7] "AtlantikSolar_ProjectBrochure_websiteversion.pdf." .

[8] A. C. Marta and P. V Gamboa, "LONG ENDURANCE ELECTRIC UAV FOR CIVILIAN SURVEILLANCE MISSIONS," 2013.

[9] "Projeto de um UAV Solar de grande autonomia Luís Filipe Vicente Cândido," 2014.

[10] "Hyperion shop." [Online]. Available: http://www.hyperion-eu.com/products/product/HP-ZS3025-10. [Accessed: 28-Dec-2015].

[11] M. L. Capture, S. T. Performance, N. L. Degradation, B. S. Response, B. Range, and O. Application, "C60 SOLAR CELL C60 SOLAR CELL," pp. 3–4.

[12] "Genasun GV-10 140W 10A Solar Charge Controller with MPPT for Lithium BatteriesGenasun." [Online]. Available: http://genasun.com/all-products/solar-charge-controllers/for-lithium/gv-10-li-lithium-10a-solar-charge-controller/. [Accessed: 23-Jan-2016].

[13] "SLS APL 10000mAh 3S1P 11,1V 25C+/40C - Lipo Modellbau Akkus bei Stefansliposhop online kaufen." [Online]. Available: http://www.stefansliposhop.de/liposhop/SLS-Multirotor/hohe-Kapazitaeten/SLS-APL-10000mAh-3S1P-11-1V-25C-40C::1095.html. [Accessed: 11-Apr-2016].

[14] "Castle Creations | Phoenix Edge Lite Controllers." [Online]. Available: http://www.castlecreations.com/products/phoenix-edge-lite.html. [Accessed: 11-Apr-2016].

[15] "CATIA - Dassault Systèmes." [Online]. Available: http://www.3ds.com/products-services/catia. [Accessed: 27-Aug-2015].

[16] EASA, "Certification Specifications for Large Aeroplanes," *Cs-25*, no. September, p. 750, 2008.

[17] T. H. G. Megson, L. D. Landau, E. M. Lifshitz, S. Chen, G. D. Doolen, and U. Alon, *Introduction to Aircraft Structural Analysis*, vol. 35, no. 1. 2010.

[18] "ANSYS - Simulation Driven Product Development." [Online]. Available: http://www.ansys.com/. [Accessed: 23-Apr-2016].

[19] B. Kasal, "Mechanical Properties of Wood," *Encycl. For. Sci.*, pp. 1815–1828, 2000.

[20] M. Cnc and T. Cnc, "EML2322L – Design & Manufacturing Laboratory CNC Facts (Summary of CNC Machining Notes)," pp. 5–6, 1950.

[21] “G-WEIKE WK1313.” [Online]. Available: http://www.wklaser.com/index.php?m=content&c=index&f=show&catid=125&l=2&id=225. [Accessed: 11-Apr-2016].

[22] “What is Laser Cutting?” [Online]. Available: http://www.thomasnet.com/articles/custom-manufacturing-fabricating/laser-cutting-technology. [Accessed: 21-Mar-2016].

[23] “G-WEIKE LG 900N.” [Online]. Available: http://www.wklaser.com/index.php?m=content&c=index&f=show&catid=128&l=2&id=247. [Accessed: 11-Apr-2016].

[24] I. Epoxy and A. Solutions, “Epoxy Adhesive Application Guide,” *Brochure*, pp. 10–19, 2012.

[25] P. D. Sheet and P. Benefits, “SikaBlock M700,” 2013.

[26] “Wet/Hand Lay-up - Manufacturing - Guide to composite materials - NetComposites Now.” [Online]. Available: http://www.netcomposites.com/guide-tools/guide/manufacturing/wethand-lay-up/. [Accessed: 20-Apr-2016].

[27] “Nuplex - Filament Winding.” [Online]. Available: http://www.nuplex.com/composites/processes/filament-winding. [Accessed: 20-Apr-2016].

[28] “Processing Technology | Bright Composites.” [Online]. Available: http://brightcomposites.com/composite-technology/processing_technology/. [Accessed: 20-Apr-2016].

[29] “Boeing 787 Advancements - AviationKnowledge.” [Online]. Available: http://aviationknowledge.wikidot.com/aviation:boeing-787-advancements. [Accessed: 20-Apr-2016].

[30] W. G. Roeseler, B. Sarh, and M. U. Kismarton, “Composite Structures: The First 100 Years,” *16th Int. Conf. Compos. Mater.*, pp. 1–10, 2007.

[31] “Mission Analysis.” [Online]. Available: http://flightdeck.ie.orst.edu/ElectronicChecklist/HTML/mission.html. [Accessed: 25-Aug-2015].

[32] Evandro Gurgel do Amaral Valente, “COMPOSITE CONSTRUCTION OF AN UNMANNED AERIAL VEHICLE.” p. 140, 2006.

[33] W. System, “Vacuum Bagging Techniques,” *Vac. Bagging Syst.*, vol. 1, no. 2, pp. 1–56, 2009.

Appendix

A Results

A.1 Preliminary sizing

Table A.1 - Shear force and bending moment

Distance $[m]$	Shear Force $[N]$	Bending Moment $[N.m]$	Distance $[m]$	Shear Force $[N]$	Bending Moment $[N.m]$
0.05	7.38	0.14	1.25	-10.42	8.01
0.1	25.74	0.51	1.3	-10.42	7.49
0.15	25.74	0.88	1.35	-10.42	6.97
0.2	25.74	1.25	1.4	-10.42	6.45
0.25	25.74	1.62	1.45	-10.42	5.93
0.3	25.77	6.32	1.5	-10.42	5.41
0.35	26.41	7.53	1.55	-10.42	4.89
0.4	26.41	8.85	1.6	-10.42	4.37
0.45	26.41	10.17	1.65	-6.83	3.96
0.5	73.50	11.49	1.7	-6.83	3.62
0.55	73.50	12.81	1.75	-6.83	3.28
0.6	-73.50	15.47	1.8	-6.83	2.94
0.65	-10.91	14.55	1.85	-6.83	2.60
0.7	-10.91	14.01	1.9	-6.83	2.25
0.75	-10.91	13.46	1.95	-6.83	1.91
0.8	-10.91	12.92	2.0	-6.83	1.57
0.85	-10.88	12.36	2.05	-6.83	1.23
0.9	-10.88	11.82	2.1	-5.65	0.59
0.95	-10.88	11.28	2.15	-5.65	0.59
1.0	-10.88	10.73	2.2	-5.65	0.34
1.05	-10.88	10.19	2.25	-2.41	0.21
1.1	-10.88	9.64	2.3	-2.24	0.10
1.15	-10.42	9.05	2.35	-1.82	0.00
1.2	-10.42	8.53	2.362	0.00	0.00

Table A.2 - Fuselage Shear force

y[m]	A $[Pa]$	B $[Pa]$	C $[Pa]$	D $[Pa]$	E $[Pa]$	F $[Pa]$	G $[Pa]$	H $[Pa]$	I $[Pa]$	J $[Pa]$	K $[Pa]$	L $[Pa]$
0	0	0	0	0	0	0	0	0	0	0	0	0
0.05	0	-1.07E+05	-1.45E+05	-1.58E+05	-1.45E+05	-1.07E+05	0	1.07E+05	1.45E+05	1.58E+05	1.45E+05	1.07E+05
0.1	0	-3.11E+05	-4.21E+05	-4.58E+05	-4.21E+05	-3.11E+05	0	3.11E+05	4.21E+05	4.58E+05	4.21E+05	3.11E+05
0.15	0	-2.74E+05	-3.71E+05	-4.03E+05	-3.71E+05	-2.74E+05	0	2.74E+05	3.71E+05	4.03E+05	3.71E+05	2.74E+05
0.2	0	-2.52E+05	-3.41E+05	-3.70E+05	-3.41E+05	-2.52E+05	0	2.52E+05	3.41E+05	3.70E+05	3.41E+05	2.52E+05
0.25	0	-2.37E+05	-3.21E+05	-3.49E+05	-3.21E+05	-2.37E+05	0	2.37E+05	3.21E+05	3.49E+05	3.21E+05	2.37E+05
0.3	0	-2.28E+05	-3.09E+05	-3.36E+05	-3.09E+05	-2.28E+05	0	2.28E+05	3.09E+05	3.36E+05	3.09E+05	2.28E+05
0.35	0	-2.24E+05	-3.06E+05	-3.33E+05	-3.06E+05	-2.24E+05	0	2.24E+05	3.06E+05	3.33E+05	3.06E+05	2.24E+05
0.4	0	-2.11E+05	-2.90E+05	-3.17E+05	-2.90E+05	-2.11E+05	0	2.11E+05	2.90E+05	3.17E+05	2.90E+05	2.11E+05
0.45	0	-2.00E+05	-2.78E+05	-3.04E+05	-2.78E+05	-2.00E+05	0	2.00E+05	2.78E+05	3.04E+05	2.78E+05	2.00E+05
0.5	0	-6.77E+05	-9.01E+05	-9.76E+05	-9.01E+05	-6.77E+05	0	6.77E+05	9.01E+05	9.76E+05	9.01E+05	6.77E+05
0.55	0	-6.87E+05	-9.11E+05	-9.86E+05	-9.11E+05	-6.87E+05	0	6.87E+05	9.11E+05	9.86E+05	9.11E+05	6.87E+05
0.6	0	6.72E+05	8.94E+05	9.68E+05	8.94E+05	6.72E+05	0	-6.72E+05	-8.94E+05	-9.68E+05	-8.94E+05	-6.72E+05
0.65	0	9.33E+04	1.25E+05	1.36E+05	1.25E+05	9.33E+04	0	-9.33E+04	-1.25E+05	-1.36E+05	-1.25E+05	-9.33E+04
0.7	0	9.30E+04	1.25E+05	1.36E+05	1.25E+05	9.30E+04	0	-9.30E+04	-1.25E+05	-1.36E+05	-1.25E+05	-9.30E+04
0.75	0	9.43E+04	1.28E+05	1.40E+05	1.28E+05	9.43E+04	0	-9.43E+04	-1.28E+05	-1.40E+05	-1.28E+05	-9.43E+04
0.8	0	1.01E+05	1.38E+05	1.50E+05	1.38E+05	1.01E+05	0	-1.01E+05	-1.38E+05	-1.50E+05	-1.38E+05	-1.01E+05
0.85	0	1.17E+05	1.57E+05	1.71E+05	1.57E+05	1.17E+05	0	-1.17E+05	-1.57E+05	-1.71E+05	-1.57E+05	-1.17E+05
0.9	0	1.30E+05	1.74E+05	1.89E+05	1.74E+05	1.30E+05	0	-1.30E+05	-1.74E+05	-1.89E+05	-1.74E+05	-1.30E+05
0.95	0	1.47E+05	1.98E+05	2.15E+05	1.98E+05	1.47E+05	0	-1.47E+05	-1.98E+05	-2.15E+05	-1.98E+05	-1.47E+05
1	0	1.71E+05	2.31E+05	2.50E+05	2.31E+05	1.71E+05	0	-1.71E+05	-2.31E+05	-2.50E+05	-2.31E+05	-1.71E+05
1.05	0	2.05E+05	2.76E+05	2.99E+05	2.76E+05	2.05E+05	0	-2.05E+05	-2.76E+05	-2.99E+05	-2.76E+05	-2.05E+05
1.1	1.3E+06	1.4E+06	1.5E+06	1.5E+06	1.5E+06	1.4E+06	1.3E+06	1.1E+06	1.1E+06	1.0E+06	1.1E+06	1.1E+06
1.15	1.4E+06	1.5E+06	1.5E+06	1.5E+06	1.5E+06	1.5E+06	1.4E+06	1.2E+06	1.2E+06	1.2E+06	1.2E+06	1.2E+06
1.2	2.0E+06	2.0E+06	2.0E+06	2.0E+06	2.0E+06	2.0E+06	2.0E+06	1.9E+06	1.9E+06	1.9E+06	1.9E+06	1.9E+06

Table A.3 - Fuselage normal stress

y[m]	A $[Pa]$	B $[Pa]$	C $[Pa]$	D $[Pa]$	E $[Pa]$	F $[Pa]$	G $[Pa]$	H $[Pa]$	I $[Pa]$	J $[Pa]$	K $[Pa]$	L $[Pa]$
0.0	0.00	0.00	0.00	0.00	0.00	0.00	0.00	0.00	0.00	0.00	0.00	0.00
0.05	6E+04	6E+04	3E+04	0.00	-3E+04	-6E+04	-6E+04	-6E+04	-3E+04	0.00	6E+04	6E+04
0.1	1E+05	1E+05	7E+04	0.00	-7E+04	-1E+05	-1E+05	-1E+05	-7E+04	0.00	1E+05	1E+05
0.15	2E+05	2E+05	1E+05	0.00	-1E+05	-2E+05	-2E+05	-2E+05	-1E+05	0.00	2E+05	2E+05
0.2	2E+05	2E+05	1E+05	0.00	-1E+05	-2E+05	-2E+05	-2E+05	-1E+05	0.00	2E+05	2E+05
0.25	3E+05	3E+05	1E+05	0.00	-1E+05	-3E+05	-3E+05	-3E+05	-1E+05	0.00	3E+05	3E+05
0.3	1E+06	1E+06	5E+05	0.00	-5E+05	-1E+06	-1E+06	-1E+06	-5E+05	0.00	1E+06	1E+06
0.35	1E+06	1E+06	6E+05	0.00	-6E+05	-1E+06	-1E+06	-1E+06	-6E+05	0.00	1E+06	1E+06
0.4	1E+06	1E+06	6E+05	0.00	-6E+05	-1E+06	-1E+06	-1E+06	-6E+05	0.00	1E+06	1E+06
0.45	1E+06	1E+06	6E+05	0.00	-6E+05	-1E+06	-1E+06	-1E+06	-6E+05	0.00	1E+06	1E+06
0.5	2E+06	2E+06	9E+05	0.00	-9E+05	-2E+06	-2E+06	-2E+06	-9E+05	0.00	2E+06	2E+06
0.55	2E+06	2E+06	1E+06	0.00	-1E+06	-2E+06	-2E+06	-2E+06	-1E+06	0.00	2E+06	2E+06
0.6	2E+06	2E+06	1E+06	0.00	-1E+06	-2E+06	-2E+06	-2E+06	-1E+06	0.00	2E+06	2E+06
0.65	2E+06	2E+06	1E+06	0.00	-1E+06	-2E+06	-2E+06	-2E+06	-1E+06	0.00	2E+06	2E+06
0.7	2E+06	2E+06	1E+06	0.00	-1E+06	-2E+06	-2E+06	-2E+06	-1E+06	0.00	2E+06	2E+06
0.75	2E+06	2E+06	1E+06	0.00	-1E+06	-2E+06	-2E+06	-2E+06	-1E+06	0.00	2E+06	2E+06
0.8	2E+06	2E+06	1E+06	0.00	-1E+06	-2E+06	-2E+06	-2E+06	-1E+06	0.00	2E+06	2E+06
0.85	3E+06	3E+06	1E+06	0.00	-1E+06	-3E+06	-3E+06	-3E+06	-1E+06	0.00	3E+06	3E+06
0.9	3E+06	3E+06	2E+06	0.00	-2E+06	-3E+06	-3E+06	-3E+06	-2E+06	0.00	3E+06	3E+06
0.95	4E+06	4E+06	2E+06	0.00	-2E+06	-4E+06	-4E+06	-4E+06	-2E+06	0.00	4E+06	4E+06
1.0	5E+06	5E+06	3E+06	0.00	-3E+06	-5E+06	-5E+06	-5E+06	-3E+06	0.00	5E+06	5E+06
1.05	7E+06	7E+06	4E+06	0.00	-4E+06	-7E+06	-7E+06	-7E+06	-4E+06	0.00	7E+06	7E+06
1.1	6E+06	6E+06	3E+06	0.00	-3E+06	-6E+06	-6E+06	-6E+06	-3E+06	0.00	6E+06	6E+06
1.15	6E+06	6E+06	3E+06	0.00	-3E+06	-6E+06	-6E+06	-6E+06	-3E+06	0.00	6E+06	6E+06
1.2	2E+06	2E+06	8E+05	0.00	-8E+05	-2E+06	-2E+06	-2E+06	-8E+05	0.00	2E+06	2E+06

Table A.4 - Empennage support shear force

y[m]	A $[Pa]$	B $[Pa]$	C $[Pa]$	D $[Pa]$	E $[Pa]$	F $[Pa]$	G $[Pa]$	H $[Pa]$	I $[Pa]$	J $[Pa]$	K $[Pa]$	L $[Pa]$
2.1	9.11E+06	9.45E+06	9.57E+06	9.61E+06	9.57E+06	9.45E+06	9.11E+06	8.77E+06	8.64E+06	8.60E+06	8.64E+06	8.77E+06
2.15	1.02E+07	1.05E+07	1.06E+07	1.07E+07	1.06E+07	1.05E+07	1.02E+07	9.83E+06	9.70E+06	9.65E+06	9.70E+06	9.83E+06
2.2	9.14E+06	9.48E+06	9.61E+06	9.65E+06	9.61E+06	9.48E+06	9.14E+06	8.80E+06	8.67E+06	8.63E+06	8.67E+06	8.80E+06
2.25	5.43E+06	5.50E+06	5.54E+06	5.56E+06	5.54E+06	5.50E+06	5.43E+06	5.35E+06	5.31E+06	5.29E+06	5.31E+06	5.35E+06
2.3	4.85E+06	4.92E+06	4.96E+06	4.97E+06	4.96E+06	4.92E+06	4.85E+06	4.78E+06	4.74E+06	4.73E+06	4.74E+06	4.78E+06

Table A.5 - Empennage support normal stress

y[m]	A $[Pa]$	B $[Pa]$	C $[Pa]$	D $[Pa]$	E $[Pa]$	F $[Pa]$	G $[Pa]$	H $[Pa]$	I $[Pa]$	J $[Pa]$	K $[Pa]$	L $[Pa]$
2.1	5.66E+06	5.66E+06	2.83E+06	0.00	-2.83E+06	-5.66E+06	-5.66E+06	-5.66E+06	-2.83E+06	0.00	5.66E+06	5.66E+06
2.15	7.67E+06	7.67E+06	3.84E+06	0.00	-3.84E+06	-7.67E+06	-7.67E+06	-7.67E+06	-3.84E+06	0.00	7.67E+06	7.67E+06
2.2	6.55E+06	6.55E+06	3.28E+06	0.00	-3.28E+06	-6.55E+06	-6.55E+06	-6.55E+06	-3.28E+06	0.00	6.55E+06	6.55E+06
2.25	6.76E+06	6.76E+06	3.38E+06	0.00	-3.38E+06	-6.76E+06	-6.76E+06	-6.76E+06	-3.38E+06	0.00	6.76E+06	6.76E+06
2.3	1.75E+06	1.75E+06	8.76E+05	0.00	-8.76E+05	-1.75E+06	-1.75E+06	-1.75E+06	-8.76E+05	0.00	1.75E+06	1.75E+06

A.2 FEM

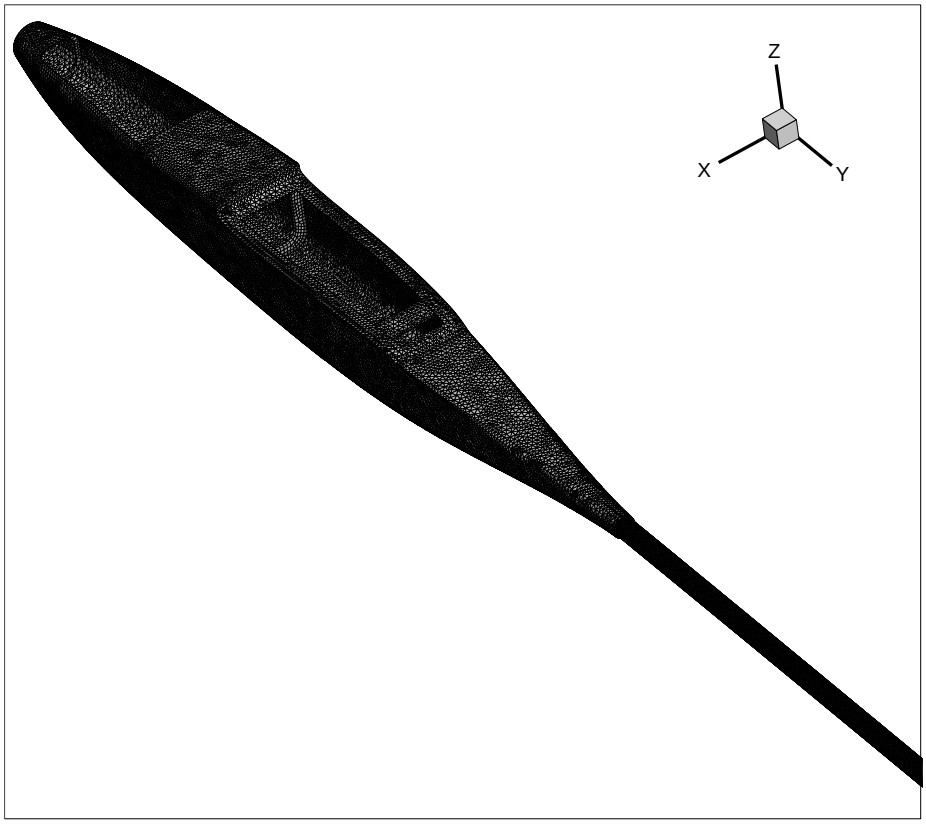

Figure A.1 - Fuselage and tail tube mesh.

The Figure A.2 explains the method used: A grey is the force and in black the frame force. This forces are only to understand the method utilized, the scale and position aren't correct.

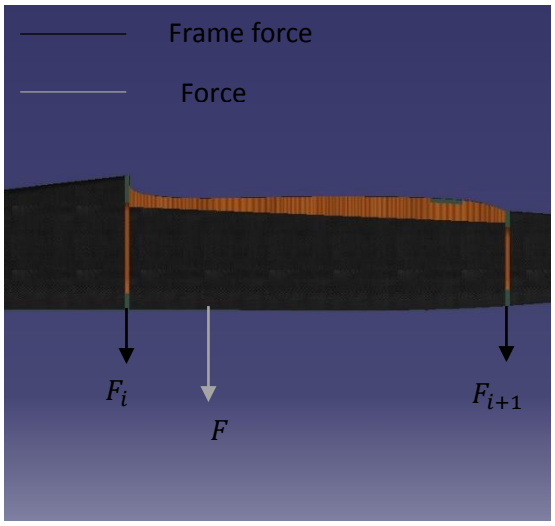

Figure A.2 - Fuselage forces.

B. Material properties

B.1 CNC

Table B.6 – CNC machining features.

Material	Spindle Speed [rpm]	Cutting Feed Rate [mm/min]	Plunging Feed Rate [mm/min]
SikaBlock®	1500	1200	800
Polystyrene foam	2000	2500	1400